Neutron and x-ray scattering for studies of biological systems

Tatiana Murugova

murugova@jinr.ru

Frank Laboratory of Neutron Physics
Joint Institute for Nuclear Research

International School on Nuclear Methods and Applied Research in Environmental, Material and Life Sciences (NUMAR-2024)
Varadero, Cuba: February 25-28, 2024

Outline

- Historical Overview: X-ray
- X-ray Sources
- Historical Overview: Neutrons
- Neutron Sources
- X-ray vs Neutron
- Theory of scattering from matter
- Imaging Techniques
- Protein crystallography
- Small angle scattering
- Other scattering methods

The Wave Nature of Light

1678 - Christiaan Huygens published Traité de la Lumière (Treatise on light). Wave theory of light
1801 - Thomas Young presented a famous paper to the Royal Society entitled "On the Theory of Light and Colours“
1818 - Augustin-Jean Fresnel theory of the light diffraction

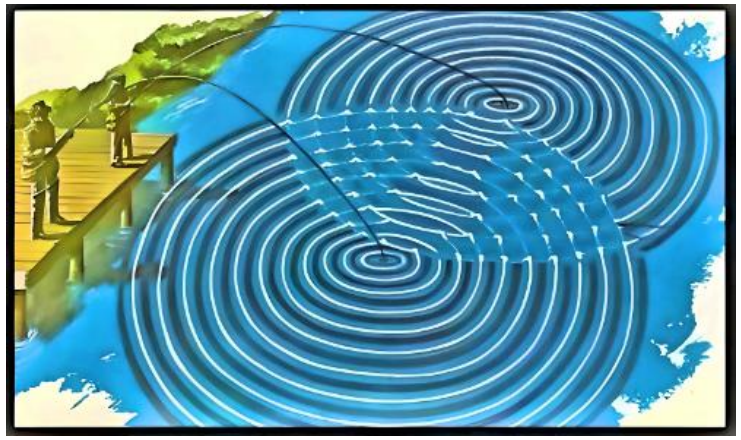

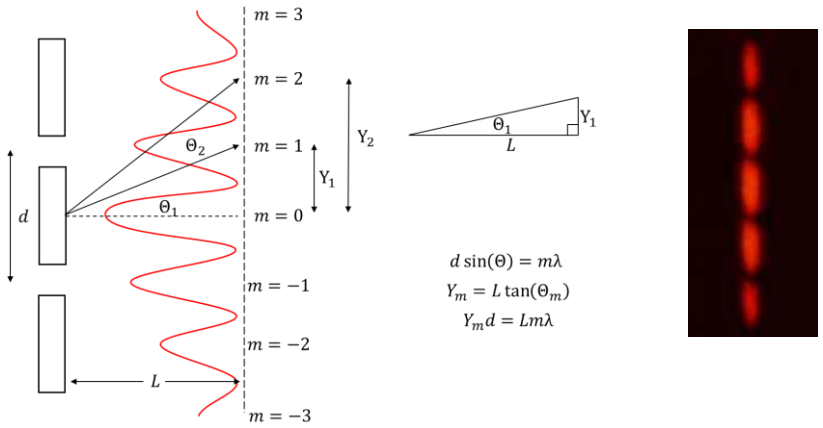

T. Young`s double-slit experiment (1801)

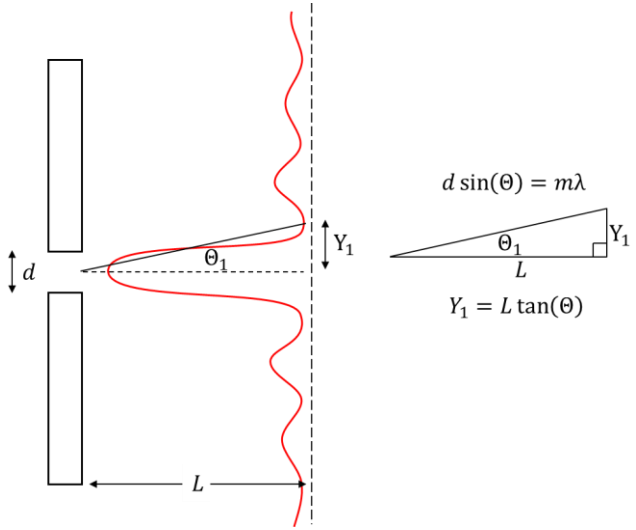

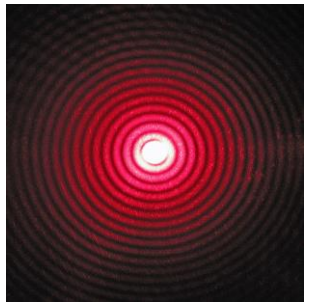

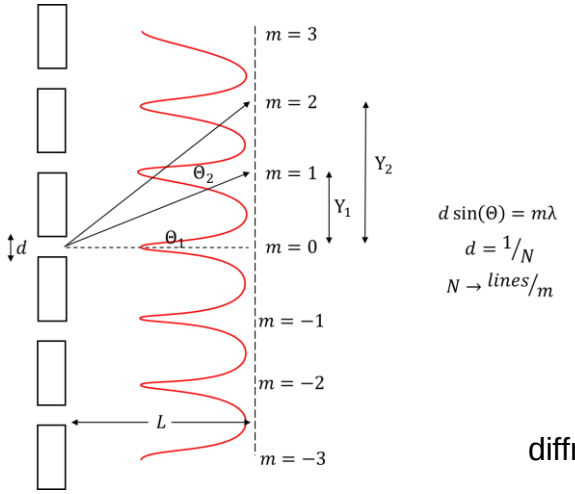

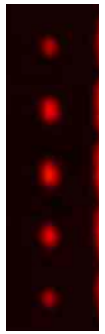

diffraction on the grating

What are x-rays?

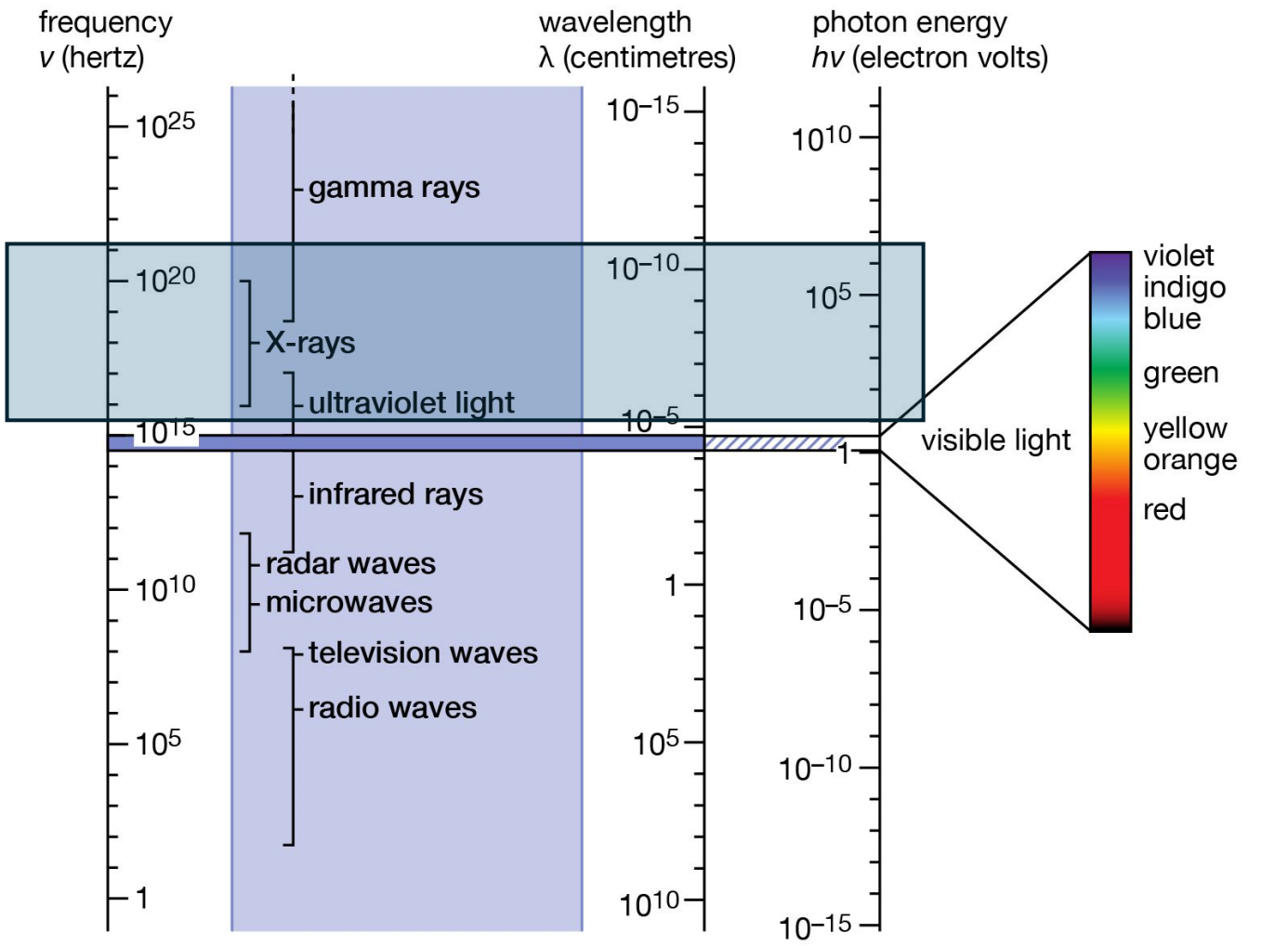

Discovery and Utilization of X-rays

1895 – Wilhelm Röntgen discovered X-rays. While experimenting with electric current flow in a partially evacuated glass tube, he noted that a radiation was emitted that affected photographic plates and caused a fluorescent substance across the room to emit light.

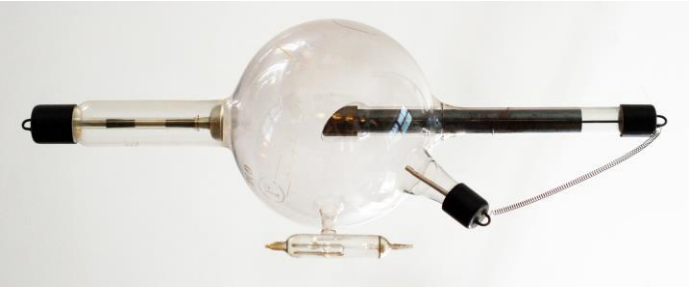

Crookes tube from early 1900s

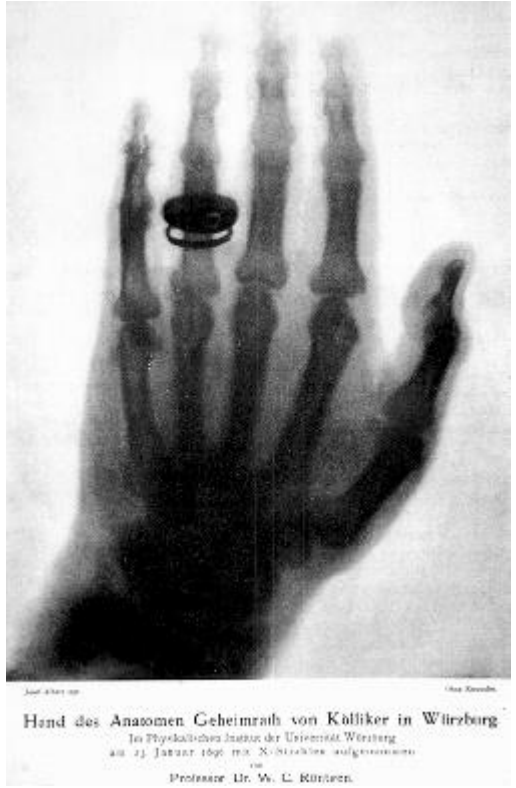

Discovery and Utilization of X-rays

1912 - the first observations of X-ray crystal diffraction by **W. Friedrich, P. Knipping** and **von Laue**.

1912—1915 W. H. Bragg , W. L. Bragg, G. Wulff interpreted diffraction in terms of reflection from crystal planes. They solved the crystal structures of NaCl and KCl and introduced Fourier analysis of the X-ray measurements.

1920s Diffraction at complex **organic crystals** (long-chain hydrocarbons, hexamethylbenzene, urea), **hairs**, **wool** fibers.

1930 - Diffraction on **nerve fibers** at different humidities.

Late **1930s - Andre Guinier** developed his theory to show that X-ray scattering at small angles, around the direct beam direction, by non-crystalline solids and solutions contained information on particle size and shape.

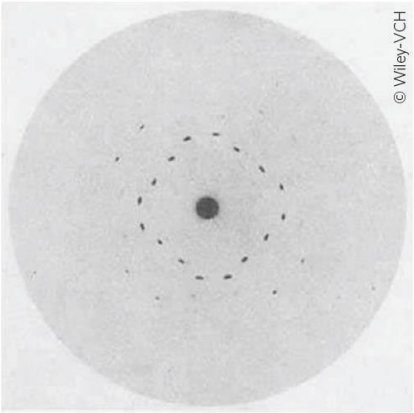

X-ray diffraction pattern from a zinc-blende (ZnS) crystal. Figure reprinted with permission from W. Friedrich *et al.* *Annalen der Physik* **346,** 971–988 (1913).

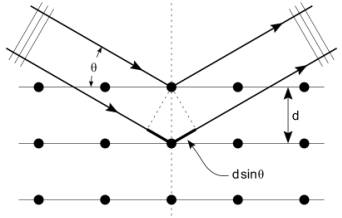

Bragg-Wulff equation:

$$2 \cdot d \sin(\theta) = n\lambda$$

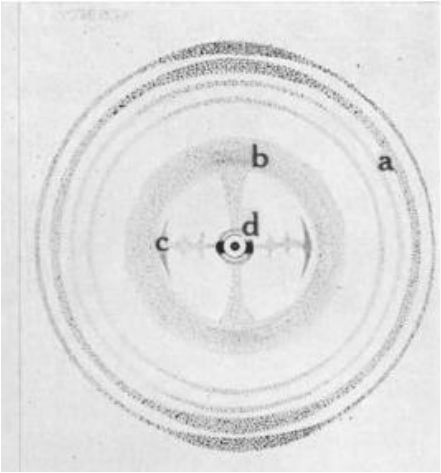

Schmitt, Francis O.; Bear, Richard S.; Clark, George L. . (1935). X-ray Diffraction Studies on Nerve. Radiology, 25(2), 131–151.

Fig. 41. Scattering pattern of uniform spherical particles (Dow Latex) obtained with a point-focusing monochromator (Fig. 32). The first visible ring is the fifth maximum (Fig. 6); on the original film, the rings are visible up to the seventeenth maximum. Sample-to-film distance: 66 cm. Cu $K\alpha$ radiation. Exposure time: 129 hours. (Danielson, Shenfil, and DuMond [25].)

Zaccai, N. R., Serdyuk, I. N., & Zaccai, J. (2017). Methods in Molecular Biophysics: Structure, Dynamics, Function for Biology and Medicine (2nd ed.). Cambridge: Cambridge University Press.

1953 - **F. Crick, J. Watson, R. Franklin and M. Wilkins** published the double-helix structure of DNA calculated from X-ray fibre diffraction and chemical model building.

7.1 A.1 Rosalind Franklin's and Maurice Wilkins' investigation of DNA structure by X-ray diffraction

Rosalind Franklin (1950's)

- Worked with Maurice Wilkins
- X-ray crystallography = images of DNA
- Provided measurements on chemistry of DNA

James Watson & Francis Crick (1953)

- Discovered the double helix by building models to conform to Franklin's X-ray data and Chargaff's Rules.

(a) Rosalind Franklin

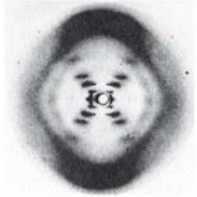

(b) Franklin's X-ray diffraction photograph of DNA

No. 4711 February 13, 1960 NATURE

1960s - Research groups led by **J. C.Kendrew and M.Perutz** published the first angstrom resolution structures of proteins (myoglobin and haemoglobin, respectively) from X-ray crystallography.

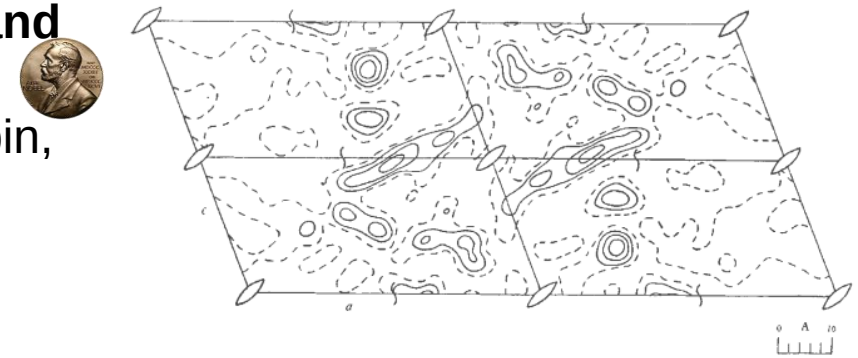

Fig. 1. Section at $y = 1/32b$. This cuts through the middle of the molecule on which the diagram is centred. 'Flat' areas indicating liquid appear on the left and right. Contours are drawn at intervals of 0·14 electron/Å.³. The broken line marks 0·4 electron/Å.³. Contours at lower levels are omitted

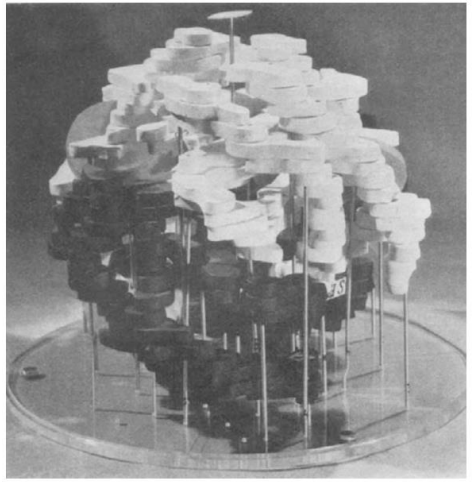

Fig. 9. Hæmoglobin model viewed normal to c

1980s - The crystallization and first X-ray crystal structures of membrane proteins were obtained by using detergents. Because they are soluble only in complex solvents, the biochemical and structural study of membrane proteins lagged far behind that of water-soluble proteins.

X-ray Sources

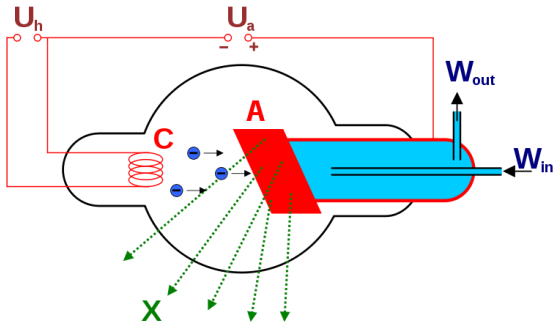

X-RAY TUBE

Decelerating electron

1895- Wilhelm Conrad Röntgen investigated the external effects from the newly developed types of vacuum Crookes tube equipment

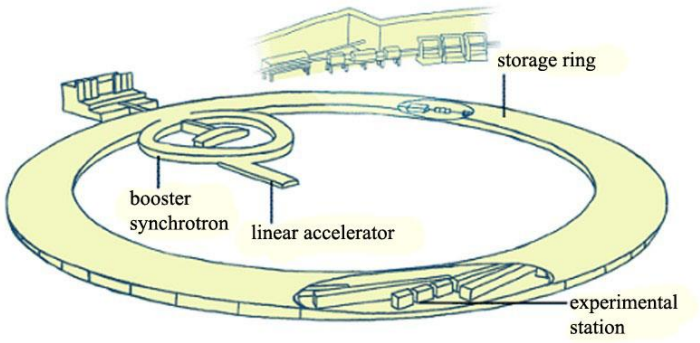

SYNCHROTRON

Accelerating electron

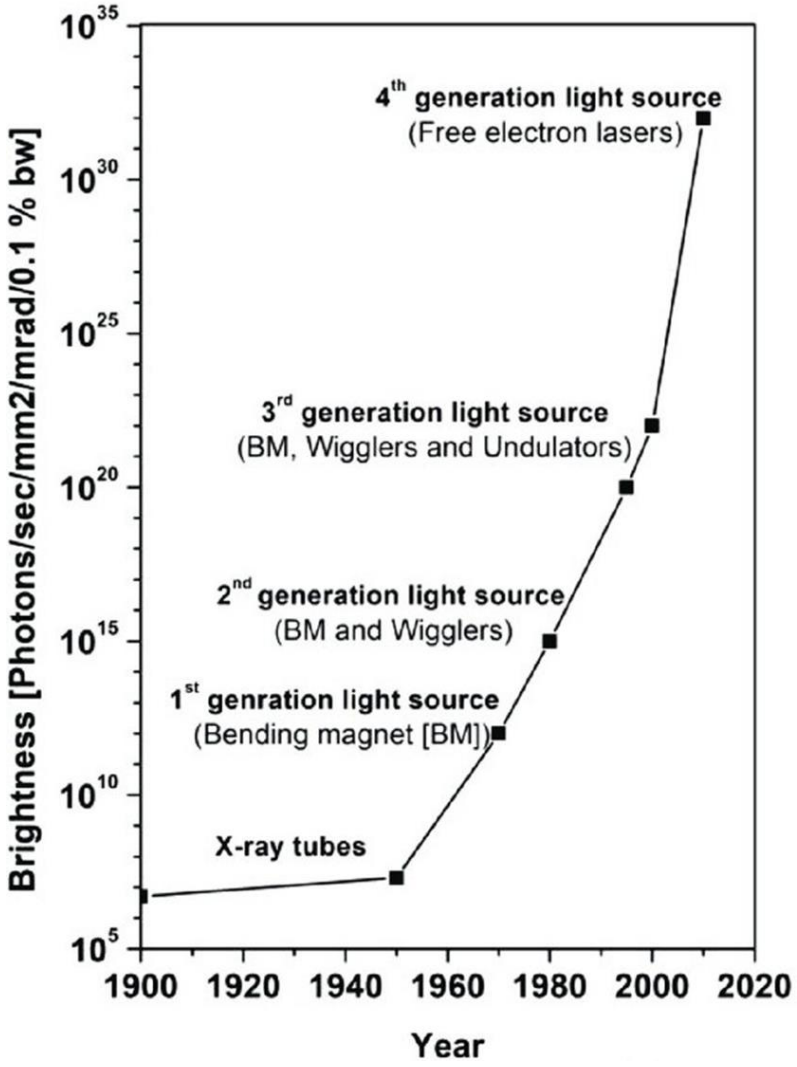

1947 – Elder, Gurewitsch, Langmuir and Pollock – observation of synchrotron radiation

1961 – Synchrotron Ultraviolet Radiation Facility at NIST – the first generation synchrotron

Bharti A, Goyal N. Fundamental of Synchrotron Radiations. Synchrotron Radiation - Useful and Interesting Applications; 2019.

X-ray scattering station at FLNP JINR, Dubna

Discovery and Utilization of Neutrons

1932 – James Chadwick - discovery of neutron

1936 - W. M. Elsasser, H. v. Halban & P. Preiswerk and D. P. Mitchell & P. N. Powers demonstrated diffraction of neutrons from a radium--beryllium source, and thus their **wave nature.**

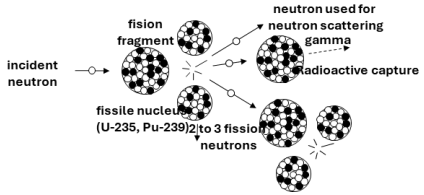

1933 – Leó Szilárd – the idea of nuclear chain reaction

1937 – Glenn T. Seaborg – concept of nuclear spallation

1942 – Enrico Fermi – the first artificial nuclear reactor Chicago Pile-1

1950-1954 – Ernest O. Lawrence – the first spallation source Materials Testing Accelerator

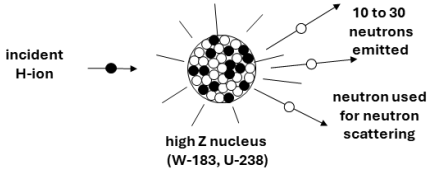

1945 and the following years
Neutron beams became available for diffraction experiments and crystallography.
C. Shull - the first **neutron diffraction** experiments
In the early 1950s, B. N. Brockhouse - the triple-axis spectrometer and measured **vibrations** in solids by neutron scattering.

1960s and 1970s
Neutron sources with neutron beams for the study of matter and biological membranes and macromolecules

C.G. Shull

Neutrons show where atoms are

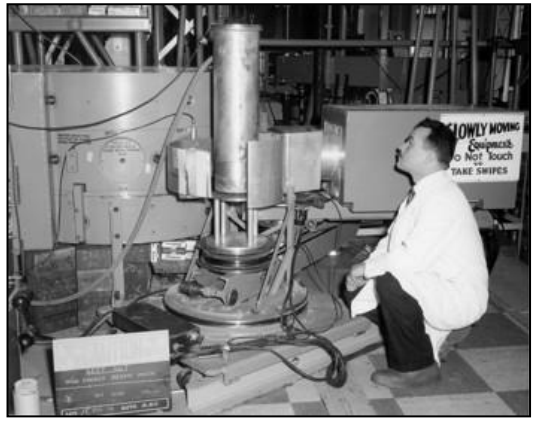

B.N. Brockhouse

Neutrons show what atoms do

1994 - "for pioneering contributions to the development of neutron scattering techniques for studies of condensed matter"

Neutron Sources

1. Continuous Reactors

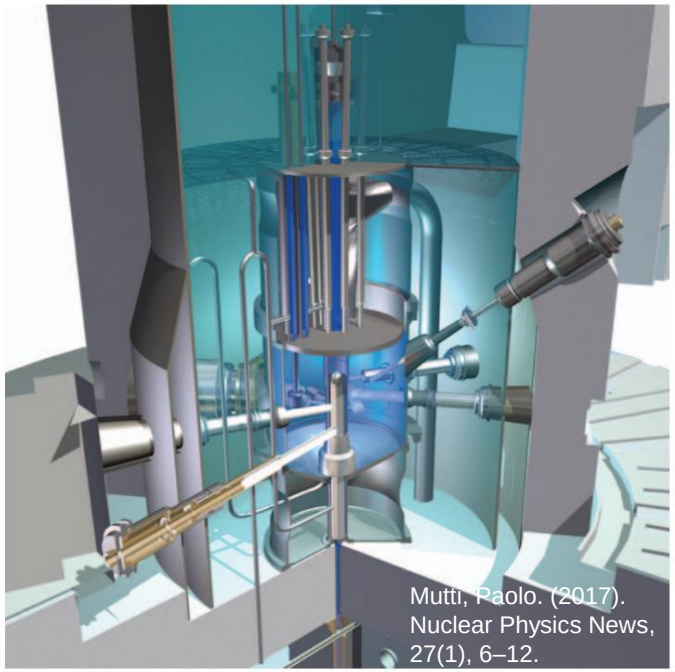

ILL High-flux Reactor, Grenoble, France

1933 – Leó Szilárd – the idea of nuclear chain reaction

1947-1993 & 1957 – National Research eXperimental & National Research Universal reactors

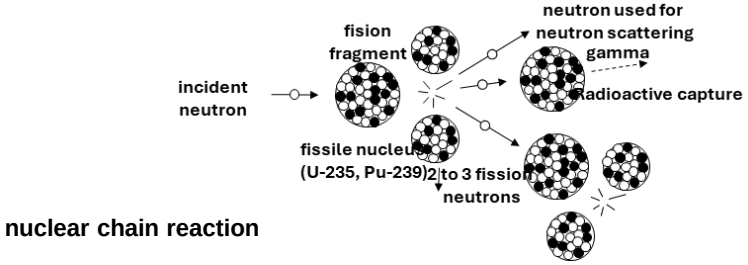

2. Spallation sources

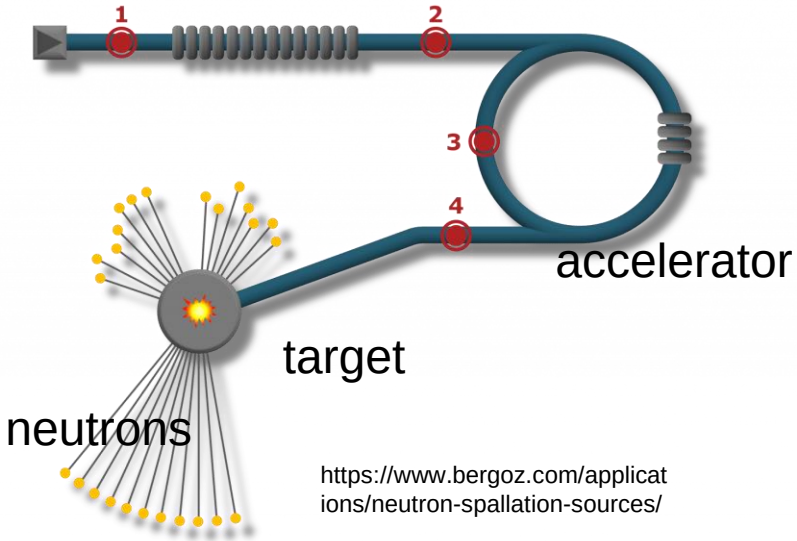

https://www.bergoz.com/applications/neutron-spallation-sources/

1937 – Glenn T. Seaborg – concept of nuclear spallation

1950-1954 – Ernest O. Lawrence – the first spallation source Materials Testing Accelerator

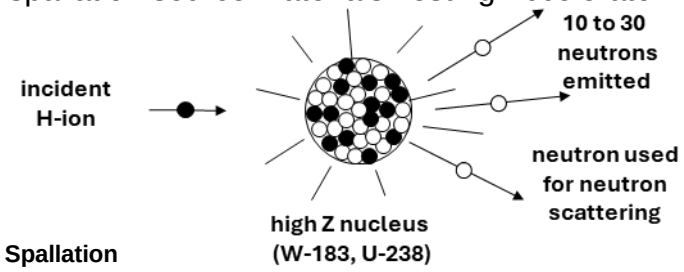

3. Pulsed Reactors

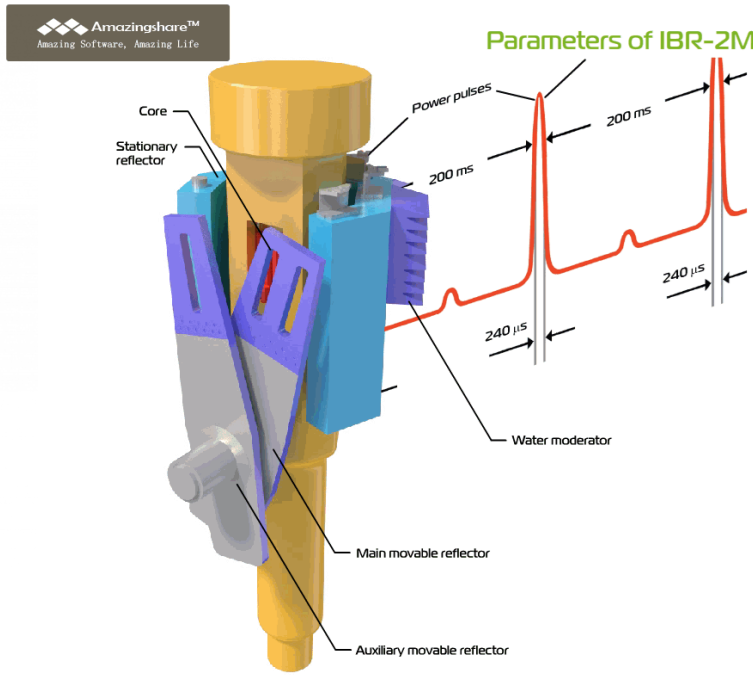

IBR-2 fast neutron pulse reactor (with a periodic operation), Dubna, Russia

1955 – Dimitry I. Blokhintsev – the idea of pulsed reactor

1960 – Ilya M. Frank & Fyodor L. Shapiro – the pulsed reactor IBR

Continuous Reactors

$\lambda = const$

Pulsed sources
Time of flight technique (TOF)

$$\lambda = \frac{h}{mv} = \frac{t \cdot h}{m \cdot L}$$

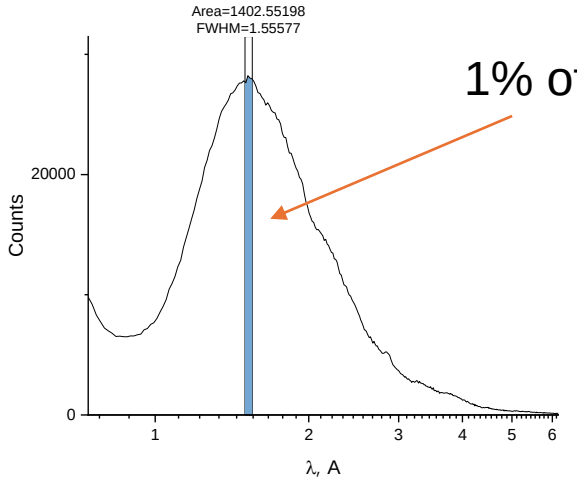

1% of neutrons

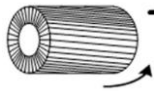

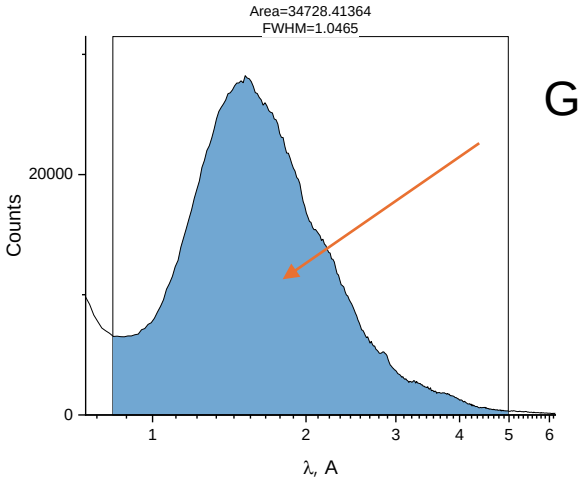

Gain is up to 90-100 %

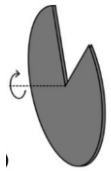

Dynamic range

$$\frac{q_{max}}{q_{min}} = \frac{\theta_{max}}{\theta_{min}}$$

θ=const

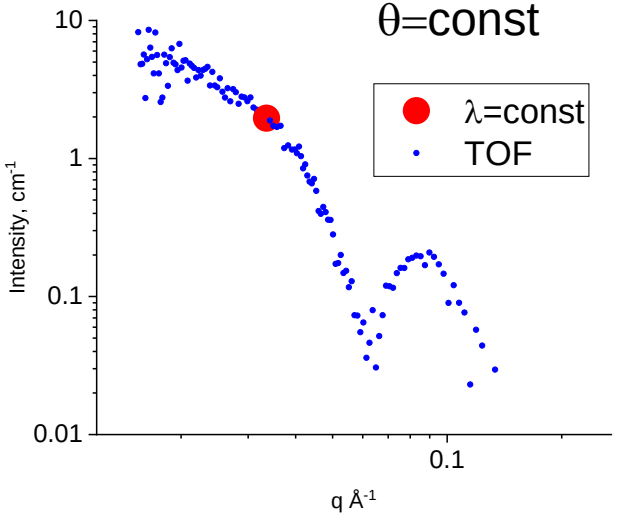

$$\frac{q_{max}}{q_{min}} = \frac{\theta_{max}}{\theta_{min}} \cdot \frac{\lambda_{max}}{\lambda_{min}}$$

Factor = 10

Scattering vector

$$q = \frac{4\pi \sin \vartheta}{\lambda}$$

X-ray and neutron characteristics

X-ray	Neutron
Scatters at the **electrons** of the atomic shell	Scattered by the **atomic nucleus**
Scattering length (“scattering power”) of an atom increases with its **number of electrons**. 	**Scattering length** shows a **random** way of nucleus dependence 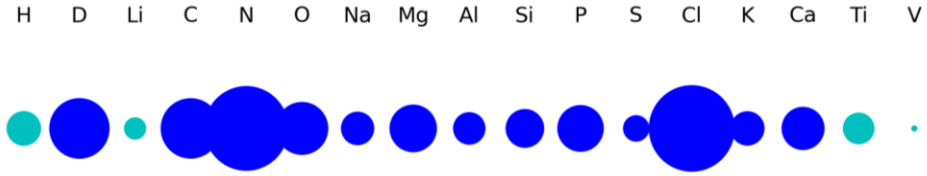
No isotope effect Heavy atoms dominate the diffraction patter	Different **isotopes** of the same element **can be very different;** hydrogen (1H) and deuterium (2H or D) is of particular interest in structural biology
λ~1Å	λ ~ 0.5-10Å
E of electrons ~10 000 eV far from movements in the matter More challenge task	Energy of movements in the matter: 10^{-9} eV – 1 eV Average E of neutrons ~0.08eV - **Ideal tool for dynamical investigations**
Researching properties of magnetic materials is more **challenge**	Spin = ½ (magnetic dipole moment) **The smallest magnetometer** 
Hight absorption by heavy elements	Deep penetration into matter
Simpler construction of sources Hight intensity	Creating neutron sources is a more difficult task

Space range of investigated objects

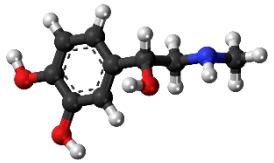

Molecules
(water, bioactive molecules, peptides, sugars etc)

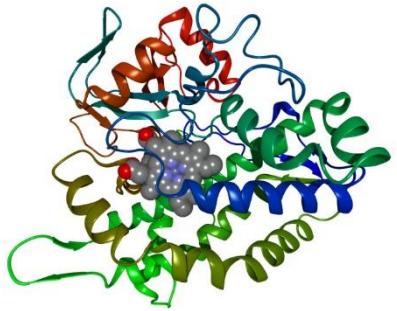

Biopolymers
(proteins, RNA, DNA, polysaccharides)

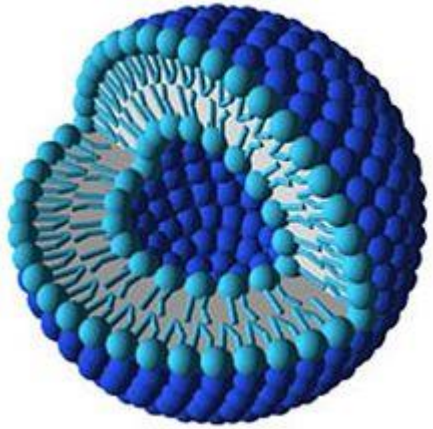

Aggregates
(micelles, model lipid and biological membranes)

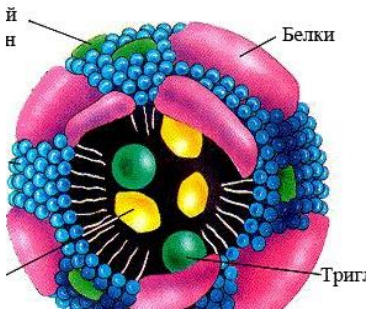

Multicomponent complex
(multi-subunit proteins, membranes, lipoproteins, fibrills, protein-DNA/RNA complexes, chromatin)

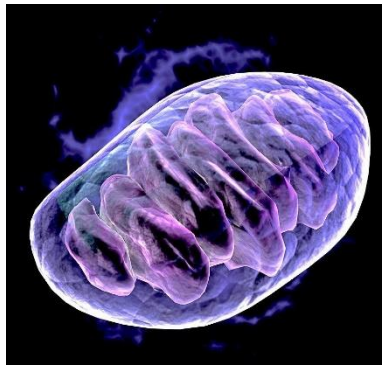

Organelles

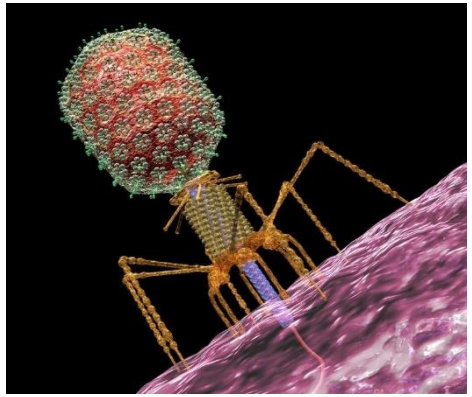

Unicellular organisms
(bacteria, viruses)

Tissues

Multicellular organisms

Time range (spectroscopy)
Dynamical properties

psec – 100 nsec

- Autocorrelation vibrations of atoms
- Substrate binding to the catalytic center, conformational changes
- Conformational mobility of subunits in protein and other macromolecular complexes (*spin-echo NSE*, ps-100ns)
- Diffusion and rotation of lipid molecules in membranes, lipid raft formation
- Membrane Undulation: physical and mechanical properties of the membrane (flexural modulus)
- Protein folding
- Dynamics of the hydration shell of macromolecules.
- Movement of water in cells (*QENS, NSE*)

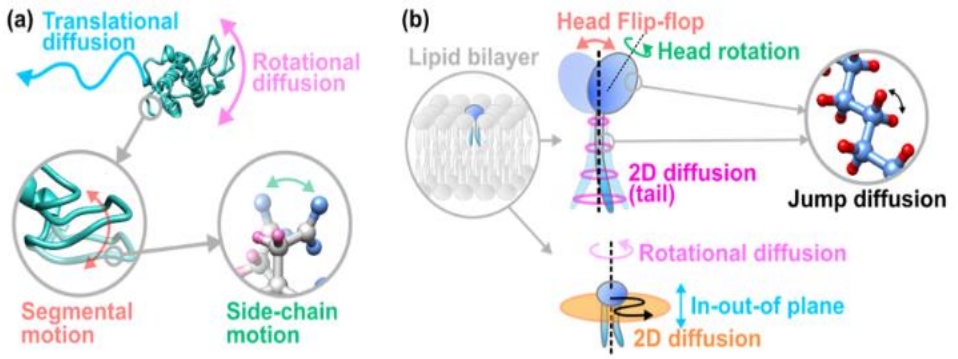

Figure 1. Hierarchical intramolecular motions observed by iNS for proteins (**a**) and lipid molecules (**b**). Classification of the motions of lipid molecules is based on the latest theoretical dynamical model called the Matryoshka model [15]. This figure is adapted from Ref. [16] with permission.

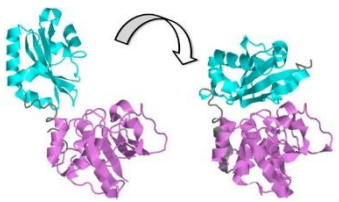

wave vector

$k_{inc} = {}^{2\pi}/_{\lambda}$

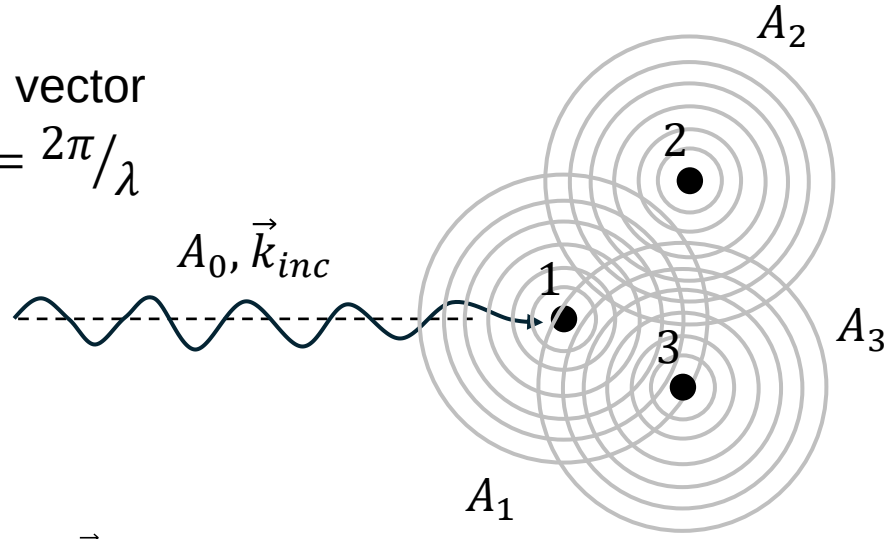

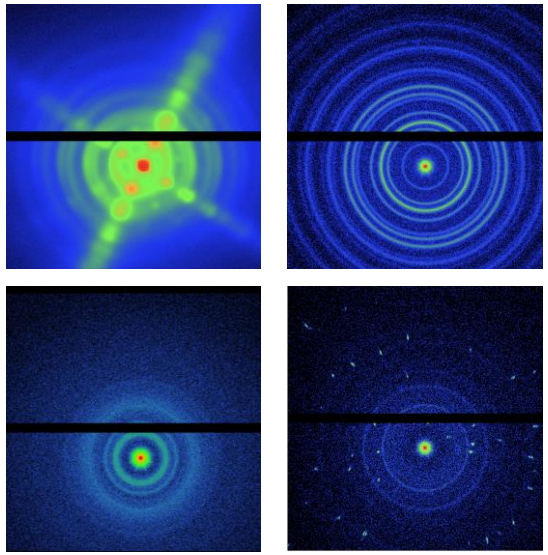

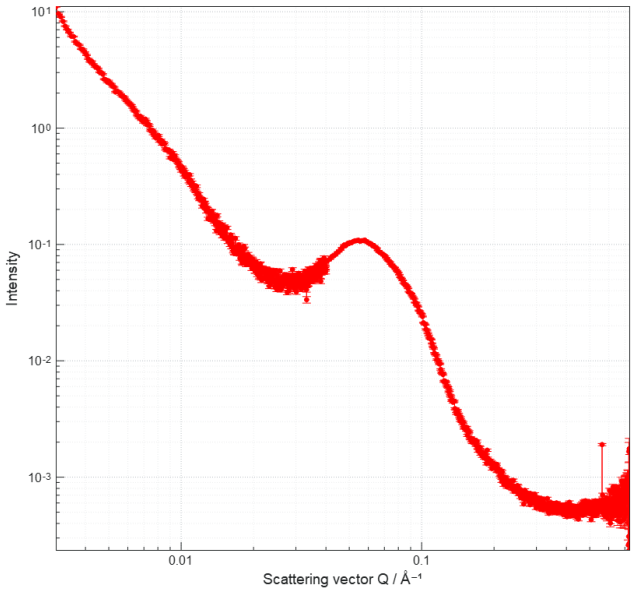

$$A_0 = e^{i\vec{k}_{inc}\vec{r}}$$

$$A_1 = A_0 b_1 \frac{e^{i\vec{k}_{sc}\vec{R}}}{|\vec{R}|}$$

$$A_2 = A_0 b_2 \frac{e^{i\vec{k}_{sc}\vec{R}}}{|\vec{R}|}$$

$$A_3 = A_0 b_3 \frac{e^{i\vec{k}_{sc}\vec{R}}}{|\vec{R}|}$$

1, 2, 3, … etc = j

$$A = A_0 e^{i\vec{k}_{inc}\vec{r}} \cdot \sum_{j=1}^{N} A_j$$

Scattering intensity

$$I(q) = \left\langle A_s(\vec{R}) \cdot A_s^*(\vec{R}) \right\rangle = \frac{A^2{}_0}{R^2} \sum_{j,k=1}^{N} b_j b_k e^{i\vec{q}(\vec{r}_j - \vec{r}_k)}$$

For continuous medium

$$I(q) = \left\langle \left| \int_V \rho(\vec{r}) e^{i\vec{q}\cdot\vec{r}} d\vec{r} \right|^2 \right\rangle$$

A – Scattering amplitude
$\vec{k} = 4\pi/\lambda$ – wave vector
b – scattering length
ρ – scattering density
$\vec{q}$ – scattering vector

Scattering vector

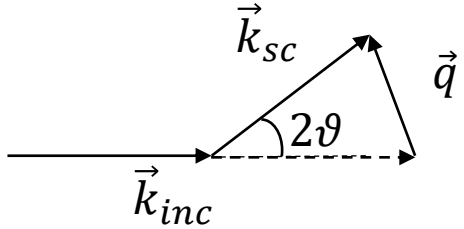

$$\rho = \frac{\sum b_i}{V}$$

$$q = \frac{4\pi \sin\vartheta}{\lambda}$$

Real space vs Reciprocal space

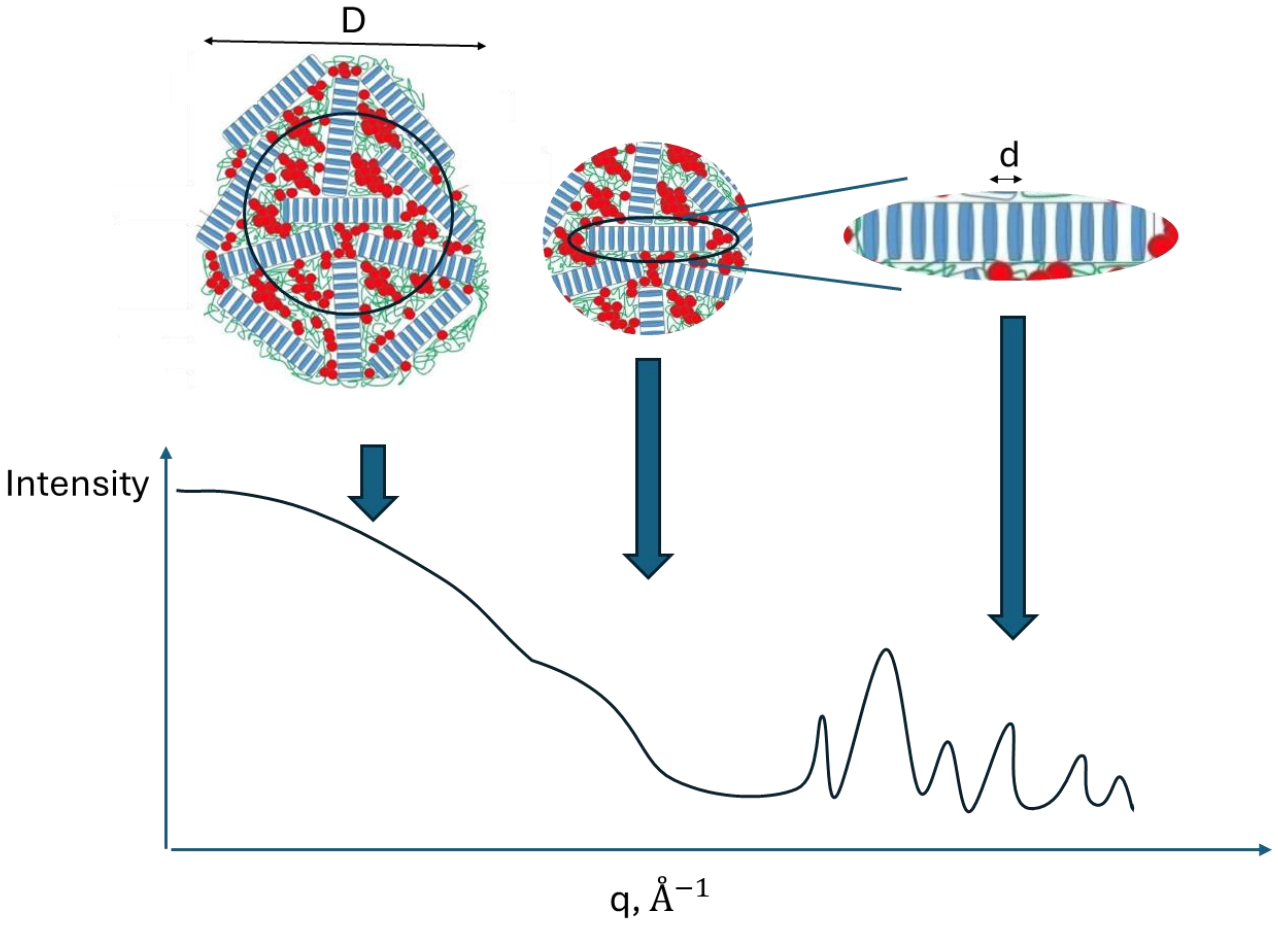

Real space

$$[D] = \frac{2\pi}{q}\,[\text{Å}]$$

Reciprocal space

$$[\text{q}] = \frac{4\pi}{\lambda}\sin\vartheta\,[\text{Å}^{-1}]$$

X-ray and neutron Imaging Techniques

X-ray – beam attenuation depends on density

Neutron - no density dependance;
- good penetration;
- direct visualization oh the hydrogen distribution

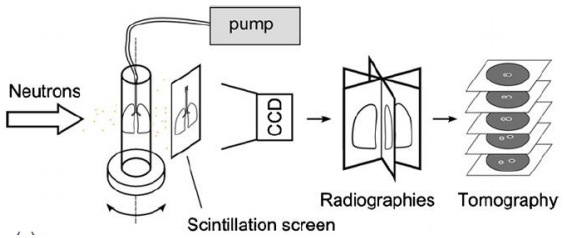

X-Ray Neutron

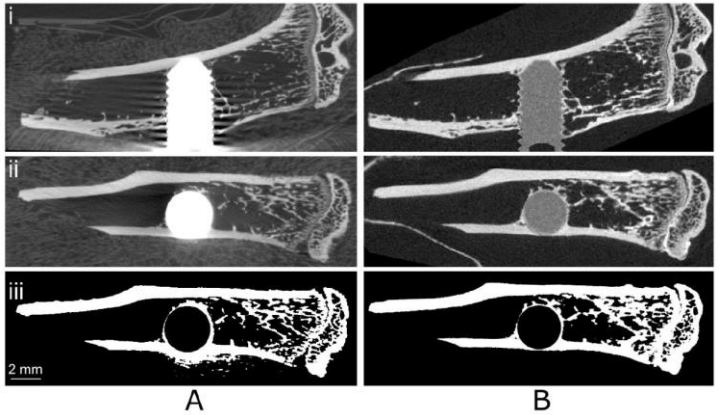

Comparison of images obtained with (A) X-ray tomography (Zeiss-XRM520 laboratory tomograph, 26 μm voxel size) and (B) neutron tomography (13.5μm voxel size)

Remodeling of bone tissue at the border with a metal implant

Hanna Isaksson, et al., Neutron tomographic imaging of bone-implant interface: Comparison with X-ray tomography, *Bone* (2017),

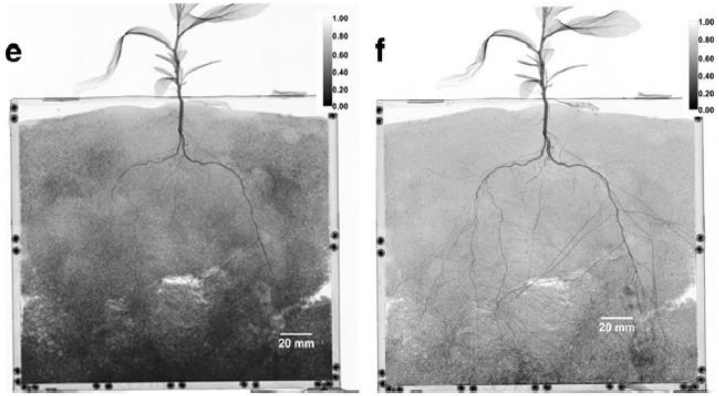

Neutron imaging.
Water distribution in newer root system: water absorption; root growth; influence of extreme drought and soil pollution.
(e) initial radiograph prior to drying cycle,
(f) final radiograph after 2-day drying cycle

Dhiman, I., *et al.* Quantifying root water extraction after drought recovery using sub-mm in situ empirical data. *Plant Soil* **424**, 73–89 (2018).

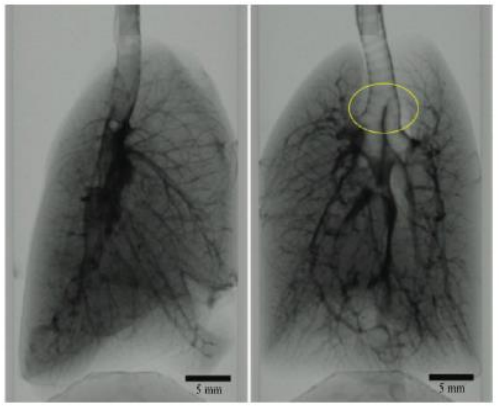

Figure 17
Left: photograph of a rat lung at the neutron beamline. Right: lateral and frontal neutron radiographs of the lung showing the lung physiology such as the trachea, lobes and airways (Metzke *et al*, 2011). The spatial resolution was approximately 50–60 μm. The yellow ellipse indicates the first bifurcation. Videos of the nCT data are available at http://iopscience.iop.org/article/10.1088/0031-9155/56/1/N01/data#.

Good contrast between air and tissue, distribution of air in the lungs. Without contrast media.

Metzke RW, et al. Neutron computed tomography of rat lungs. Phys Med Biol. 2011 Jan 7;56(1):N1-N10.

X-ray/neutron protein crystallography

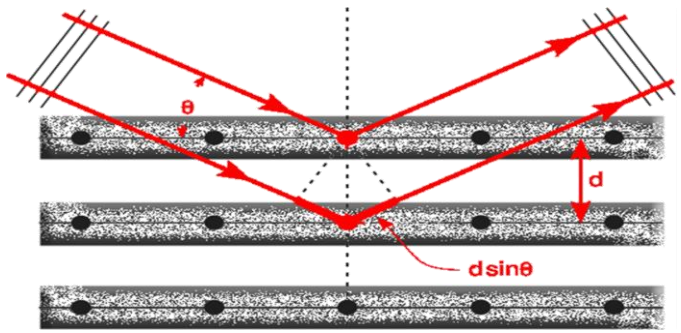

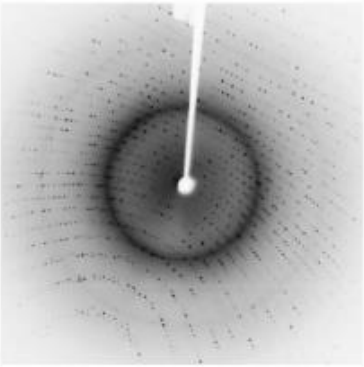

The Bragg's Law

The two planes will scatter in phase if the path difference '2 d sin(q)' is a whole number of wavelengths 'n λ':

$$2 \cdot d \sin(\theta) = n\lambda$$

Why do we need protein crystals?

1. Understanding the mechanisms of functioning of living systems at the atomic level
2. Developing drugs (Rational design)
3. Proteins – the main target for drug design

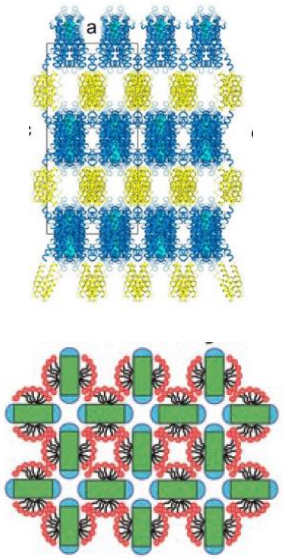

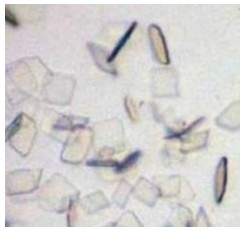

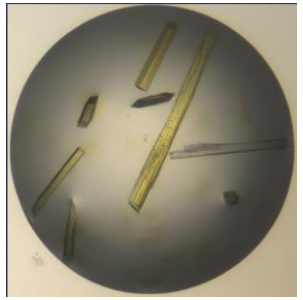

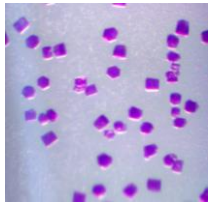

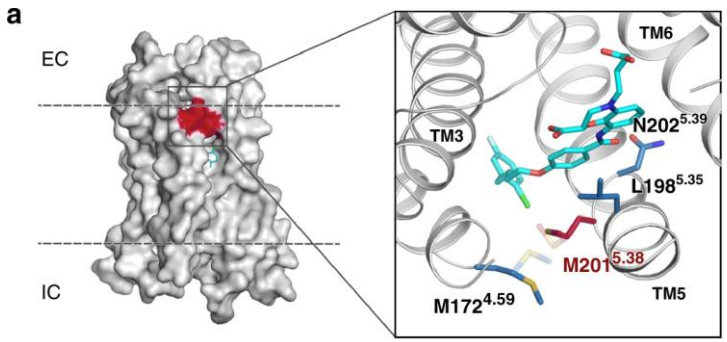

Kermani AA. FEBS J. 2021 Oct;288(20):5788-5804.

Remeeva A., et al. Proteins: Structure, function and bioinformatics (2021).

Gusach, A., Luginina, et al. Nat Commun 10, 5573 (2019).

Principle of protein crystallography

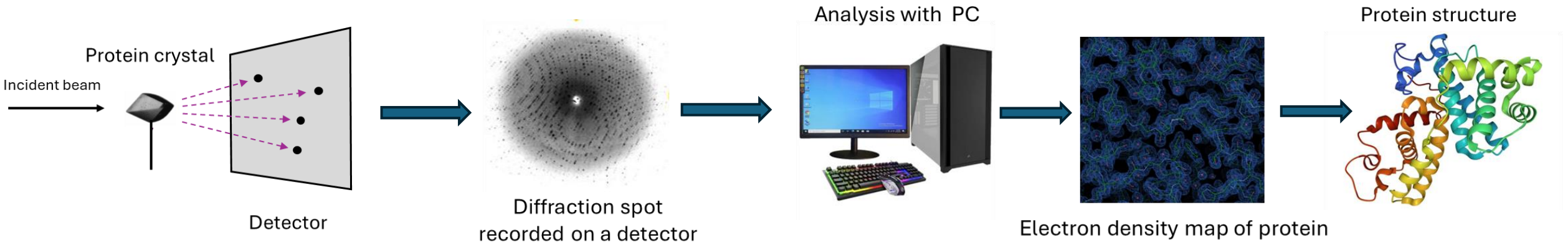

Sample preparation	Diffraction experiment	Structural analysis
Overexpression	Diffraction data collection	Calculating of electron density
Purification		Model building
Crystallization		

Advantages of neutron protein crystallography

Limits for x-ray

- **Hydrogen are invisible** by x-ray -> position of H are extrapolated from chemical knowledge
- **Radiation damage** -> artefacts. Essential for proteins contained Metals and redox –cofactors
- **Cryo-temperatures -** frozen crystals at -170 -180 oC

Advantages of neutrons

- Can see Hydrogen and Water
- Non- destructive
- Physiologically relevant temperatures

Special tasks for neutrons

- Investigation of enzyme catalytic mechanisms,
- Direct experimental insight into chemical reactions
- Mechanism of redox enzymes (no radiation damage)
- Location of hydrogen bond network governing ligand binding (e.g. pharmaceutical drugs)
- Proton transfer pathways

Problems in neutron experiments

- Growing large crystals
- Deuterating crystals (for decreasing noise)
- Long time of measuring

50% total atoms in biomolecules are HYDROGENs

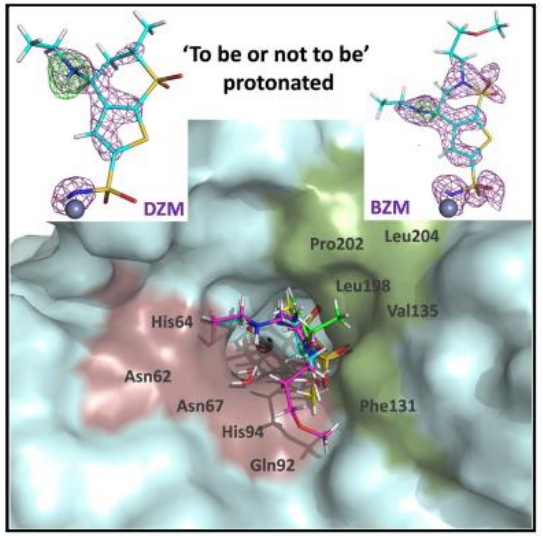

Human Carbonic Anhydrase
hCA II (15 isomers)

Catalyzes the reversible hydration of CO2.

- Glaucoma
- Epilepsy
- Altitude sickness
- Some types of cancer

The **position of hydrogen atoms** has been determined. The network of hydrogen bonds has been found; that gives the idea of introducing an additional hydrogen into drug`s structure to enhance its binding with active site.

X-ray – the tail of brinzolamide is located in a hydrophobic pocket (low temperatures)
Neutrons – in a hydrophilic pocket (room temperatures)
--> It is necessary to pay attention to hydrophilic pockets in other isomers hCA

A. Kovalevsky et al., "To Be or Not to Be" Protonated: Atomic Details of Human Carbonic Anhydrase-Clinical Drug Complexes by Neutron Crystallography and Simulation Structure, 2018, **26**, 383.

Small angle scattering

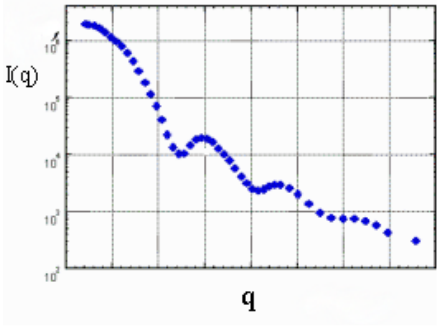

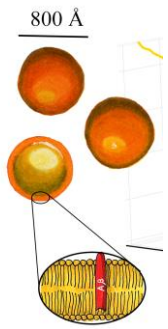

Fields

- Biology
- Colloid chemistry
- Materials Science
- Solid State
- Polymer physics

Structural information:
10-1000 Å

- Size, volume, molecular weight
- Form
- Conformation
- Oligomeric state
- 3D structures with ~10 Å resolution

Type of objects

- Solutions of macromolecules and their complexes
- Alloys
- Films
- Powders

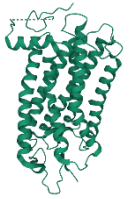

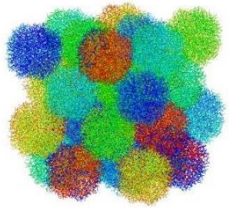

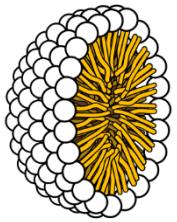

Small angle scattering experiment

Incident beam

Sample in cuvette

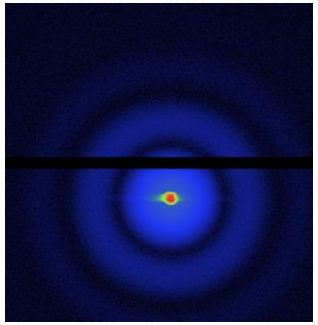

Detector

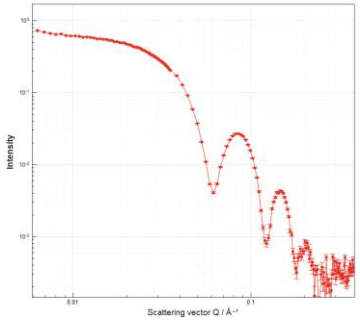

Azimuthal averaging

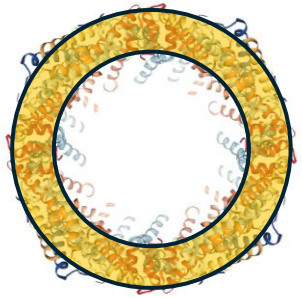

Model

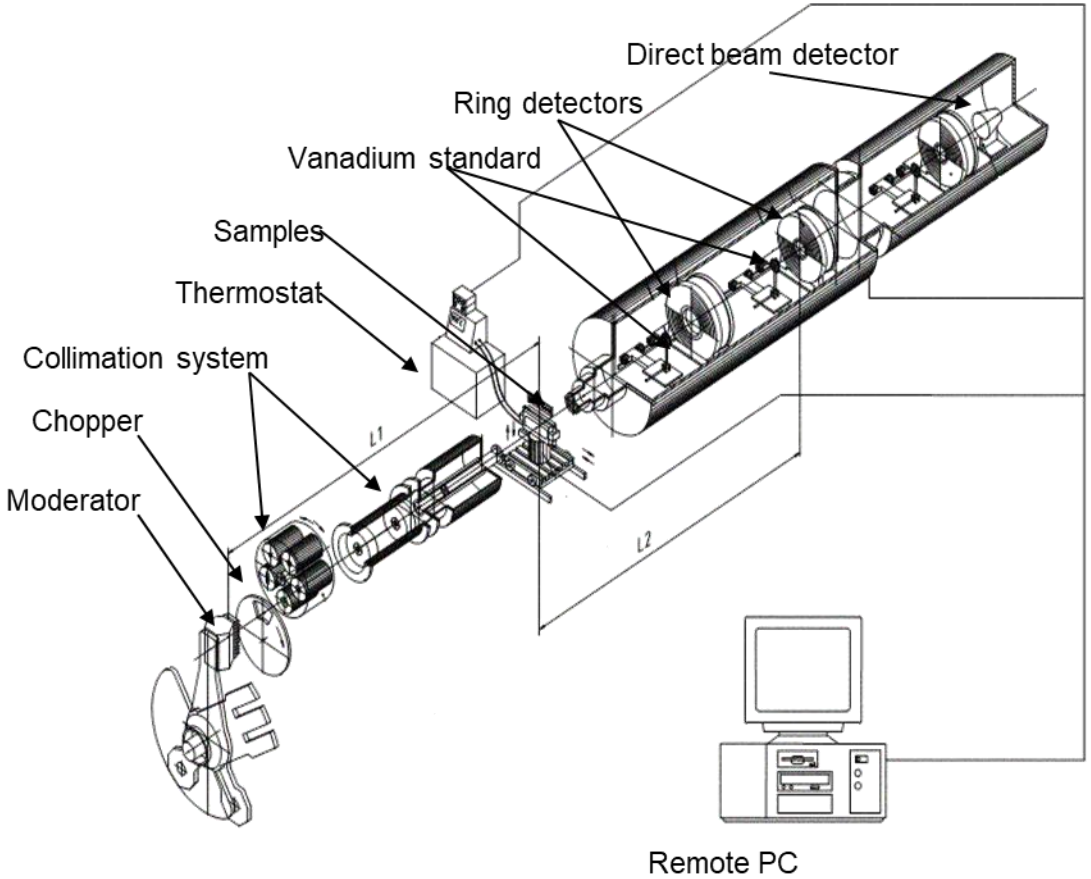

YuMO SANS-spectrometer at IBR-2 reactor, Dubna. Russia

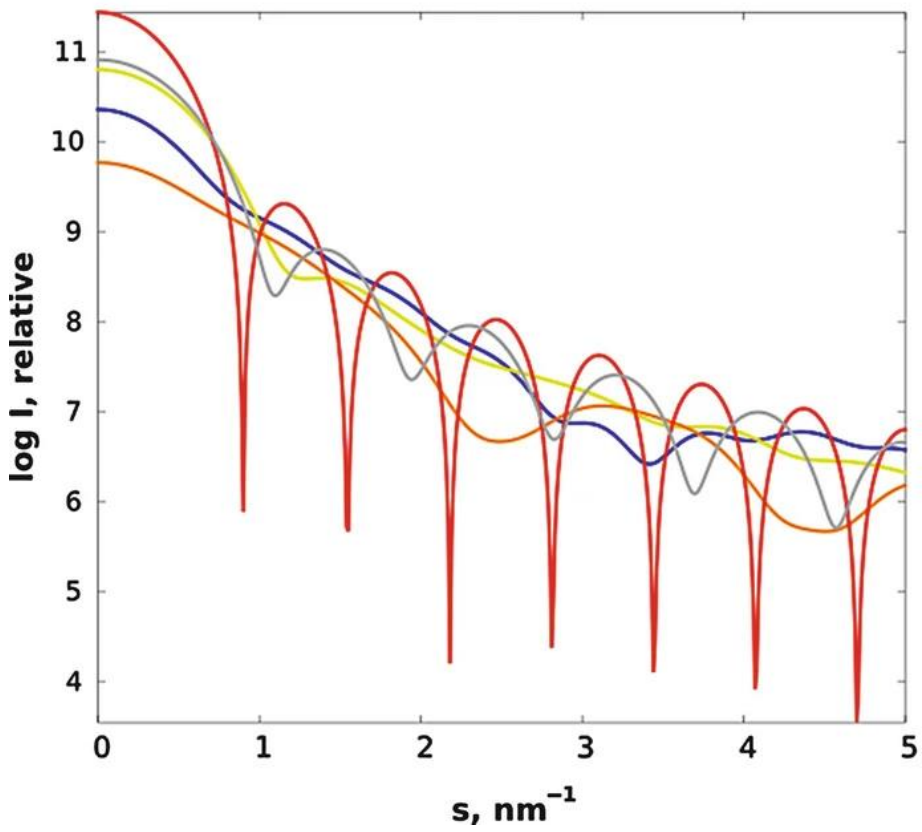

Size Shape Surface

Allec, N., Choi, M., Yesupriya, N. et al. Small-angle X-ray scattering method to characterize molecular interactions: Proof of concept. Sci Rep 5, 12085 (2015).

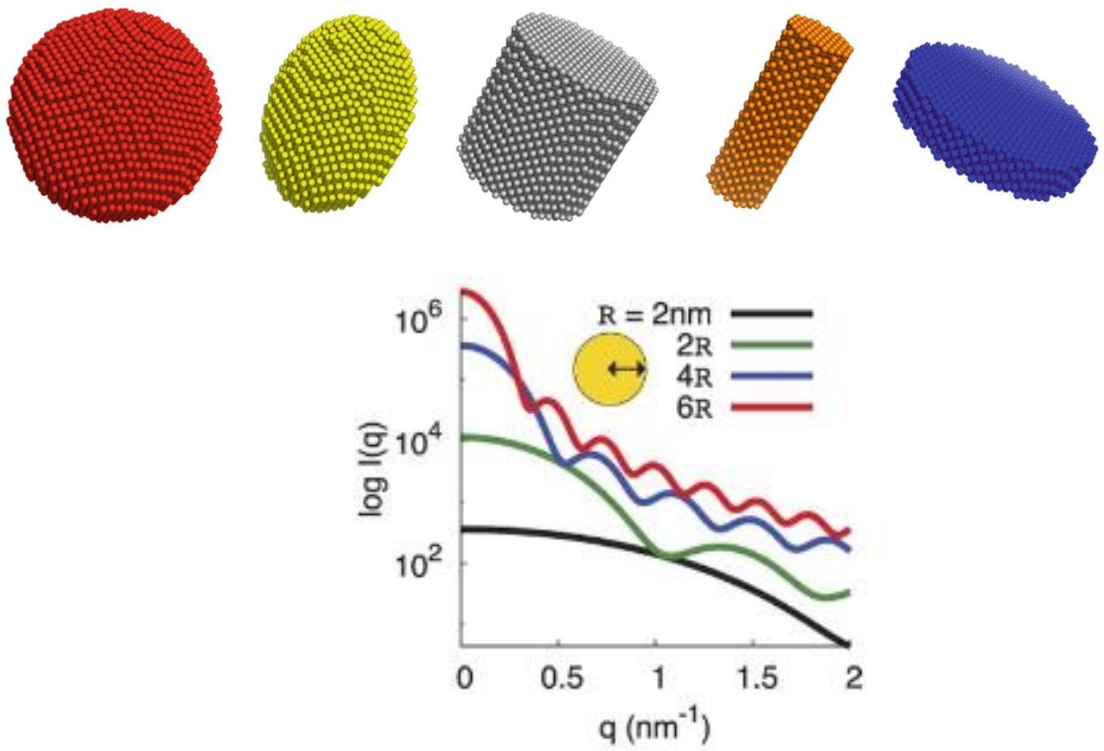

Franke, D., Svergun, D.I. (2020). Synchrotron Small-Angle X-Ray Scattering on Biological Macromolecules in Solution. In: Jaeschke, E., Khan, S., Schneider, J., Hastings, J. (eds) Synchrotron Light Sources and Free-Electron Lasers. Springer, Cham. https://doi.org/10.1007/978-3-030-23201-6_34

Guinier Regime

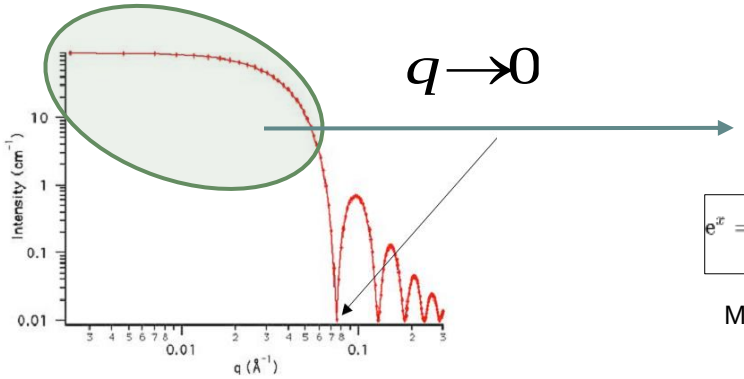

$q \to 0$

$$e^x = 1 + \frac{x}{1!} + \frac{x^2}{2!} + \frac{x^3}{3!} +$$

Maclaurin series

$$I(q) = \left| \int_V \rho(\vec{r}) e^{i\vec{q}\vec{r}} d\vec{r} \right|^2$$

$q \to 0$

$$\boxed{I(q) \sim V^2 \left[1 - \frac{q^2 R_q^2}{3!} + \right]^2 \approx V^2 e^{-\frac{q^2 R_q^2}{3}}}$$

$$I(q) = const \cdot e^{-\frac{1}{3} R_g^2 q^2}$$

$$qI(q) = const \cdot e^{-\frac{1}{2} R_g^2 q^2}$$

$$q^2 I(q) = const \cdot e^{-R_g^2 q^2}$$

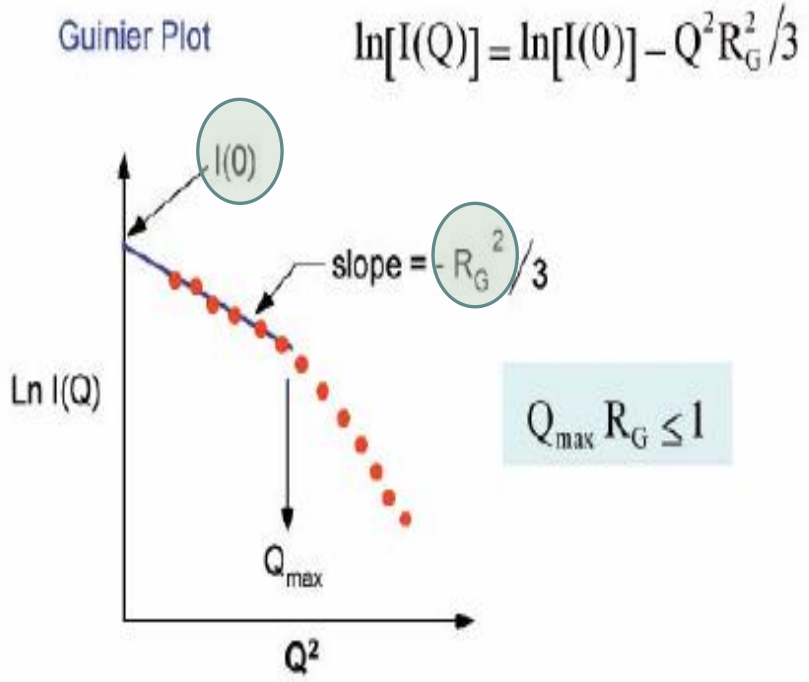

Radius of gyration
R_g^2 is the average squared distance of the scatterers from the centre of the object

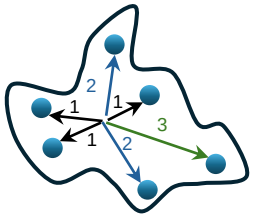

$$R_g^2 = (1^2 + 1^2 + 1^2 + 2^2 + 2^2 + 3^2)\ /6 = 20/6$$
$$R_g^2 = \sqrt{3.333} = 1.82$$

Radius of gyrations depends on particles shape

Objects	$\langle R_G^2 \rangle^{1/2}$
Sphere with a radius R	$\sqrt{\frac{3}{5}}R$
Spherical shell with an outer and inner radius of R_o and R_i, respectively	$\sqrt{\frac{3(R_o^5 - R_i^5)}{5(R_o^3 - R_i^3)}}$
Cylinder with a radius R and a length t; therefore:	$\sqrt{\frac{R^2}{2} + \frac{t^2}{12}}$
Long rod: $R \to 0$ and $t \gg R$	$\frac{t}{\sqrt{12}}$
Thin disk: $t \to 0$ and $R \gg t$	$\frac{R}{\sqrt{2}}$

Molecular mass estimation

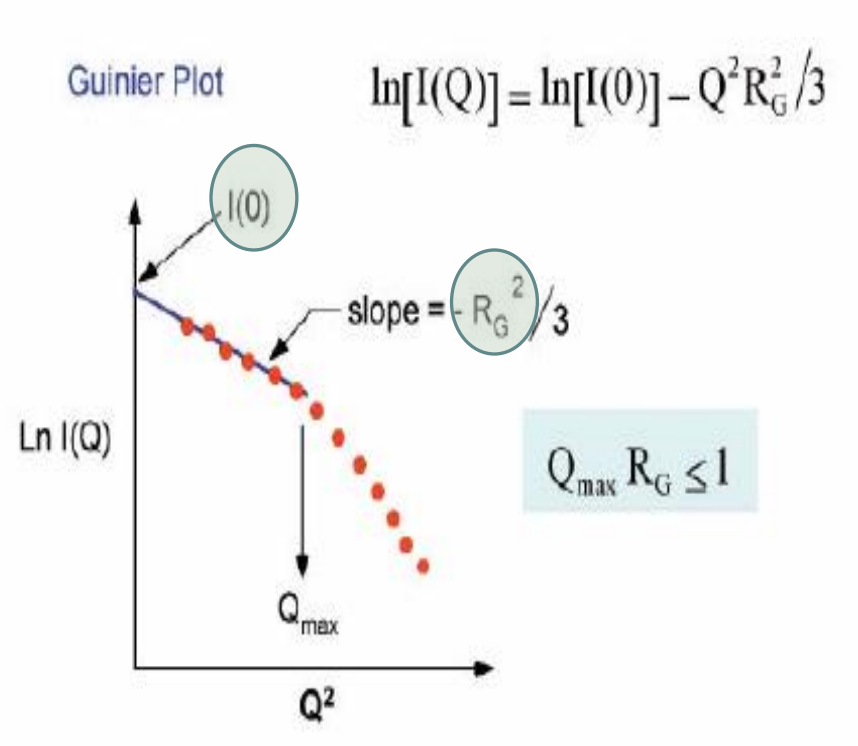

$$I(0) = \left| \int_V \rho(\vec{r}) d\vec{r} \right|^2 \xrightarrow{\rho = const} (\rho V)^2$$

Molecular weight:

$$\boxed{MW = \frac{I(0) N_A}{c(\bar{\rho} - \rho_{buffer})^2 \nu^2}}$$

N_A-Avogadro`s number

c - concentration

ρ_{buffer}-scattering density of a buffer

$\bar{\rho}$ - scattering density of a studied molecule

ν- partial specific volume, cm^3/g

Pair distance distribution function

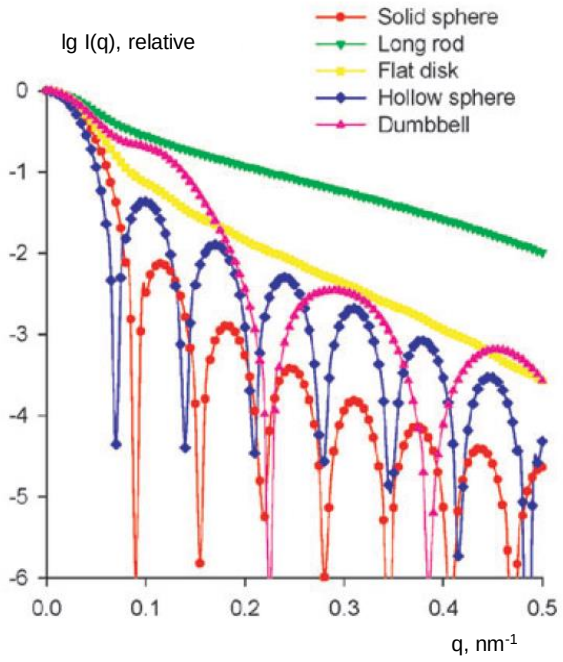

$$P(r) = \frac{r^2}{2\pi}\int_0^\infty q^2 I(q)\frac{\sin(qr)}{qr}dr$$

Fourier Transform

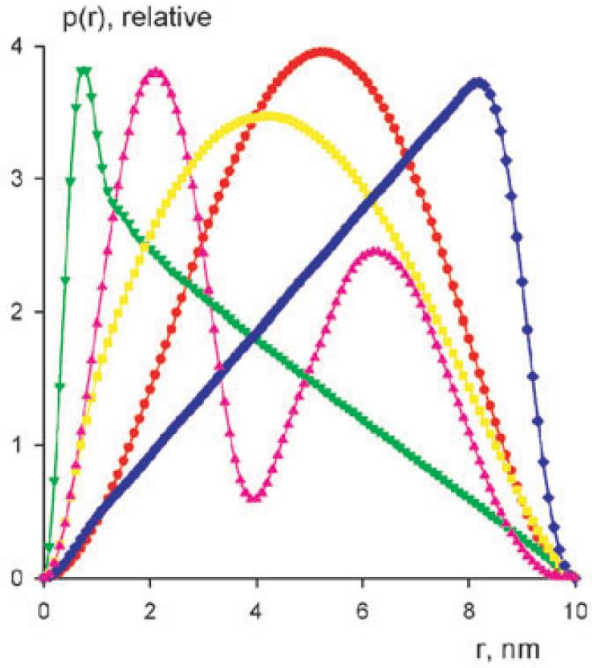

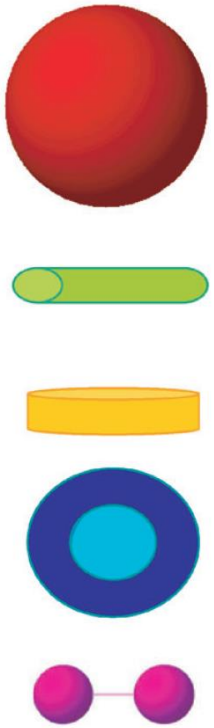

Scattering intensities of geometrical bodies with the same maximum size

distance distribution functions of geometrical bodies with the same maximum size

Blanchet CE, Svergun DI. Small-angle X-ray scattering on biological macromolecules and nanocomposites in solution. Annu Rev Phys Chem. 2013;64:37-54. doi: 10.1146/annurev-physchem-040412-110132.

Analytical functions (Form factors)

Common form factors of particulate systems

Morphologies	P(q)	Remarks
Spheres (radius :R)	$\frac{9}{(qR)^6}[\sin(qR) - qR\cdot\cos(qR)]^2 = A_{sph}^2(qR)$	• Integration of x and y are for orientational average. • $J_1(x)$ is the first kind Bessel function of order 1
Spherical shells (outer radius: R_1 inner radius: R_2)	$\frac{[R_1^3\cdot A_{sph}(qR_1) - R_2^3\cdot A_{sph}(qR_2)]^2}{(R_1^3 - R_2^3)^2}$	
Triaxial ellipsoids (semiaxes: a,b,c)	$\int_0^1\int_0^1 A_{sph}^2[q\sqrt{a^2\cos^2(\pi x/2) + b^2\sin^2(\pi x/2)(1-y^2)_1 + c^2y^2}\,]\,dx\,dy$	
Cylinders (radius: R length: L)	$4\int_0^1 \frac{J_1^2[qR\sqrt{1-x^2}\,]}{[qR\sqrt{1-x^2}\,]^2}\,\frac{\sin^2(qLx/2)}{(qLx/2)^2}\,dx$	
Disk (radius: R infinitely thin)	By setting L = 0 $\quad \frac{2 - J_1(2qR)/qR}{q^2R^2}$	
Rod (length: L infinitely thin)	By setting R = 0 $\quad \frac{2}{qL}\int_0^{qL}\frac{\sin(t)}{t}\,dt - \frac{\sin^2(qL/2)}{(qL/2)^2}$	

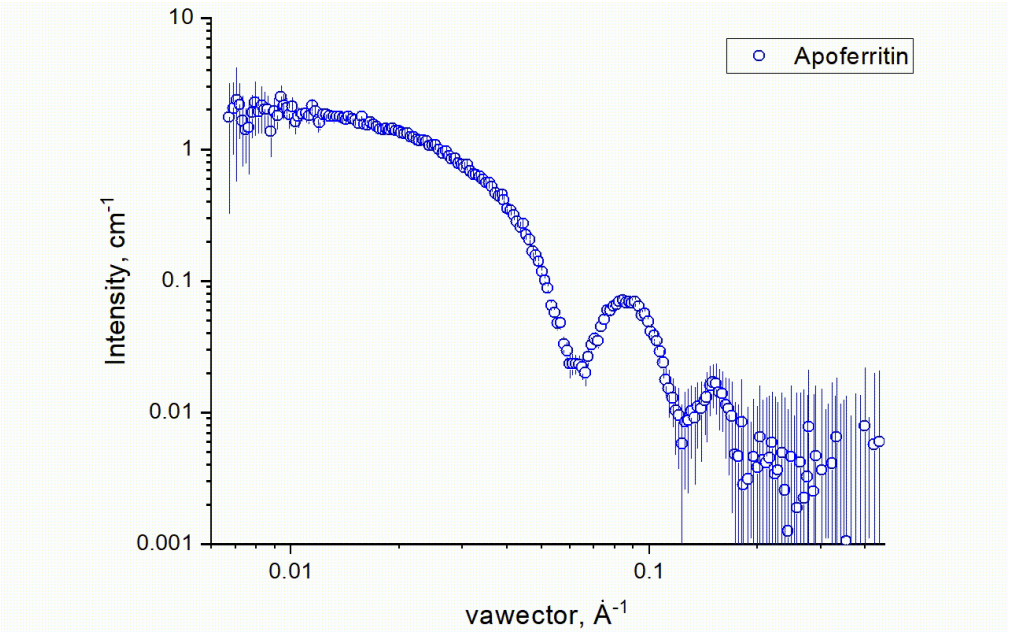

by A. Ivankov

"Structure Analysis by Small Angle X-Ray and Neutron Scattering" L. A. Feigen and D. I. Svergun

Amyloid Beta Peptide changes the morphology of lipid membrane

Small Spherical Hollow Shells

Bilayered Disks

Large Spherical Hollow Shells

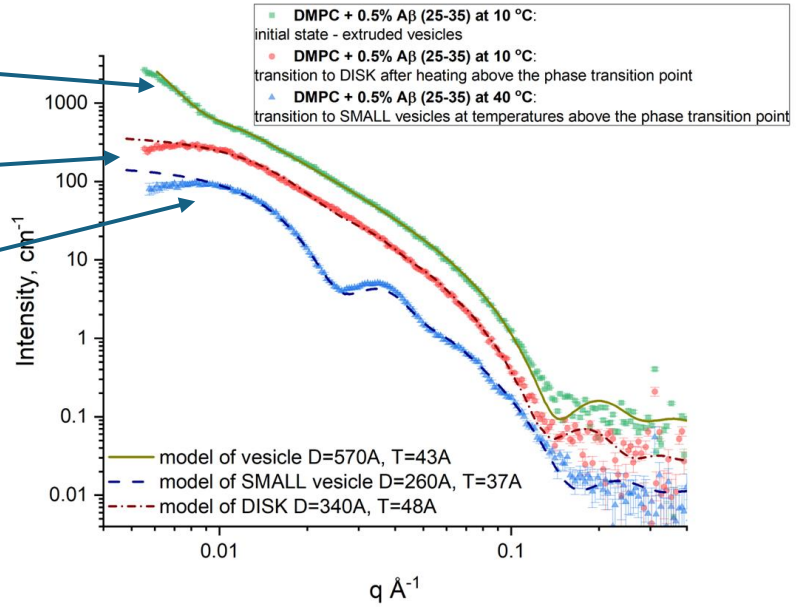

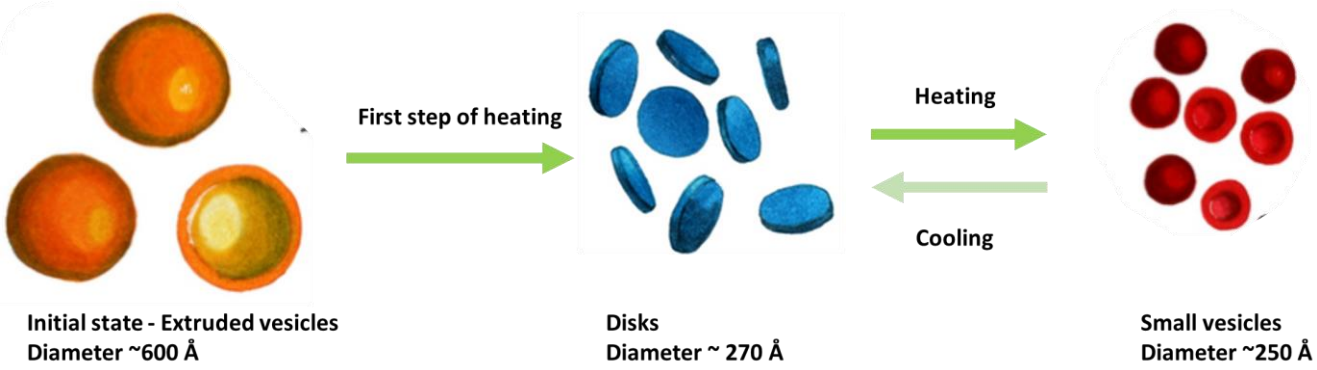

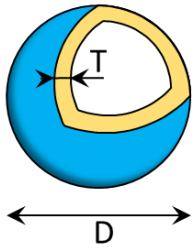

Vesicle

(Spherical Hollow Shells)

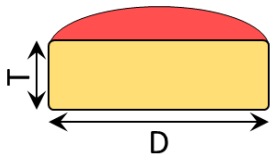

Disk

Changes in the membrane self-organization happen during the thermodynamic phase transitions of lipids and are interpreted as the peptide driven membrane breakage.

Ivankov, Murugova, Ermakova, Kondela, Badreeva, … Kučerka, Scientific Reports 11 (2021)

Ab initio modelling

Da Vela S, Svergun DI. Methods, development and applications of small-angle X-ray scattering to characterize biological macromolecules in solution. Curr Res Struct Biol. 2020 Aug 27;2:164-170. doi: 10.1016/j.crstbi.2020.08.004.

Data analysis software ATSAS 3.2.1

Debye`s formula

$$I(q) = \sum_{i=1}^{K} \sum_{j=1}^{K} f_i(q) f_j(q) \frac{\sin(qr_{ij})}{qr_{ij}}$$

K - number of beads,

$f_i(q)$- scattering amplitude from the ith dummy atom

r_{ij} – is the distance between a pair of dummy atoms.

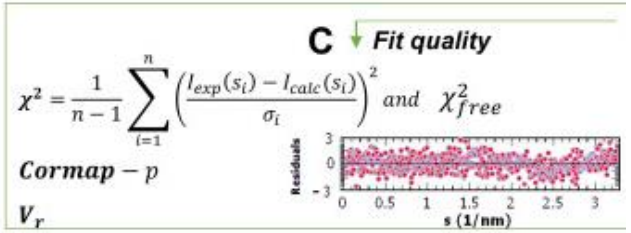

https://capsidconstructors.github.io/lab-book/saxs.html
S. Rajan et al. Sci. Rep. 5, 10609 (2015),

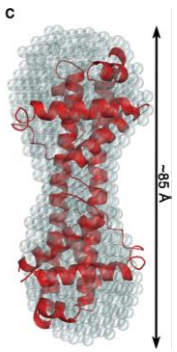

apoptosis-regulating protein

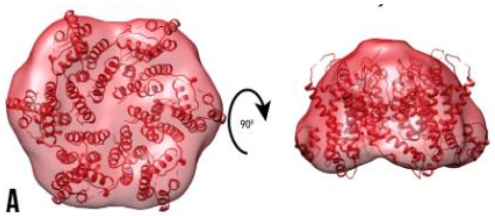

Ab initio reconstruction of HIV-1 CA hexamer overlaid with PDB ID 3H47[1]

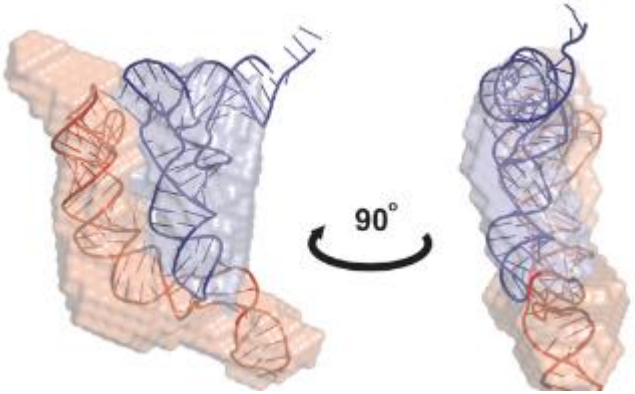

I86–tRNA complex model

Chen Y, Pollack L. s. Wiley Interdiscip Rev RNA. 2016 Jul;7(4):512-26.
Fornillos, O., et al. (2009). Capsid.*Cell*, 137(7), pp.1282-1292.

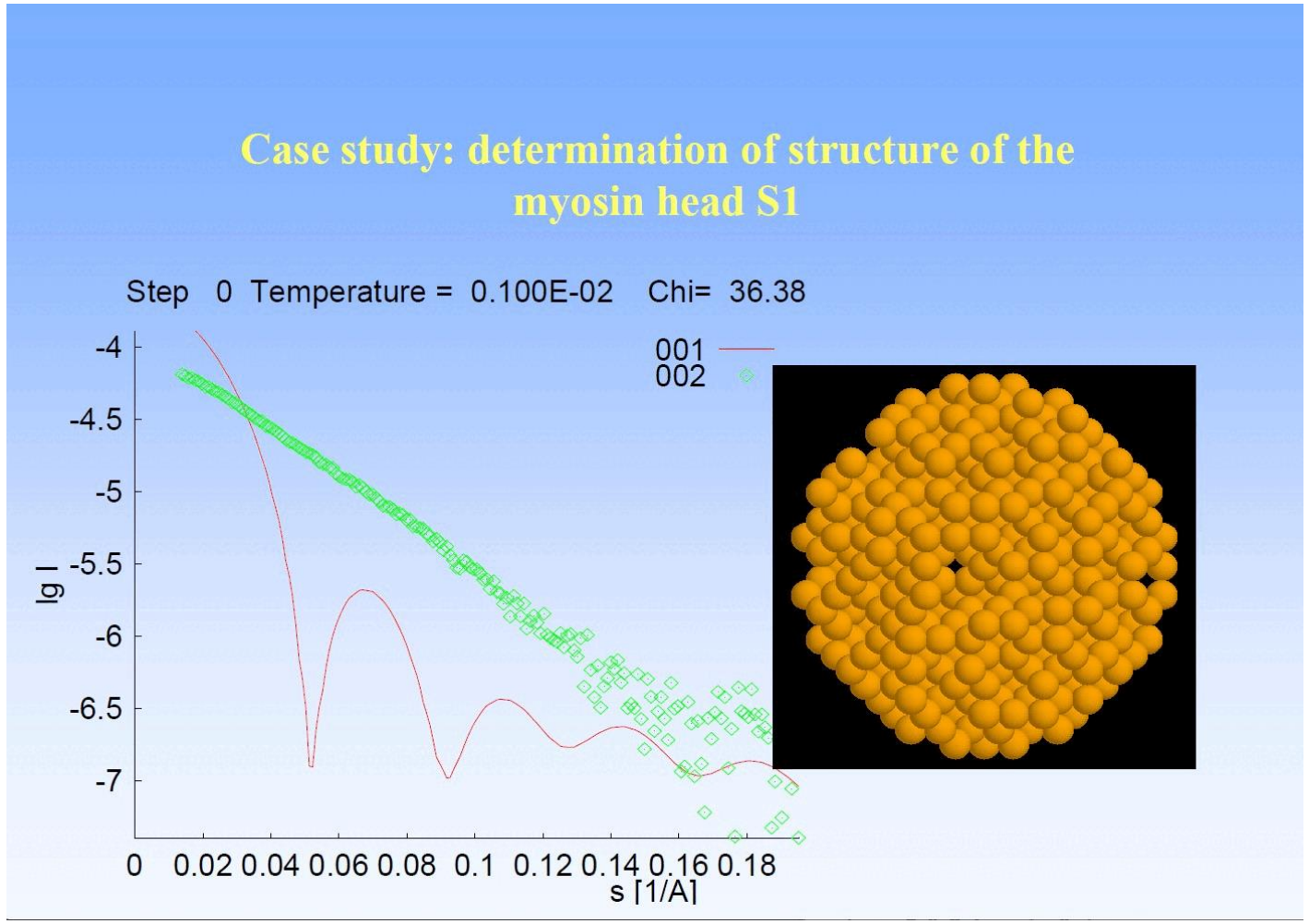

From presentation of V.V. Volkov , FSRC Crystallography & Photonics RAS, Moscow

Molecular dynamics simulations + SAS

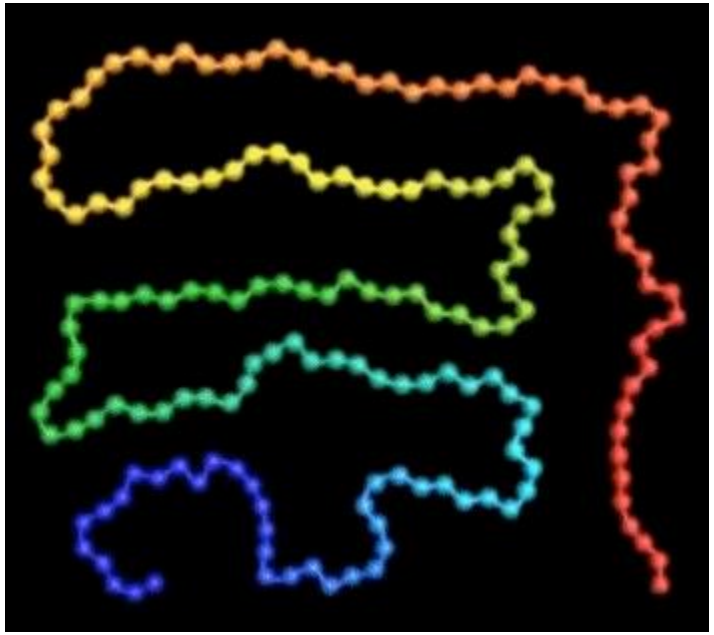

Simulation by Dina Badreeva, JINR

- The trajectories of atoms and molecules are determined by numerically solving Newton's equations of motion for a system
- Calculations use interatomic potentials or molecular mechanical force fields

Programs for I(q) calculation:
- Data analysis software ATSAS
- FoxS

https://youtu.be/yZ2aY5lxEGE?si=aHP1mb-dx3lfe5o5

Molecular model of a sensor of two-component signaling system: photoreceptor from N. pharaonis

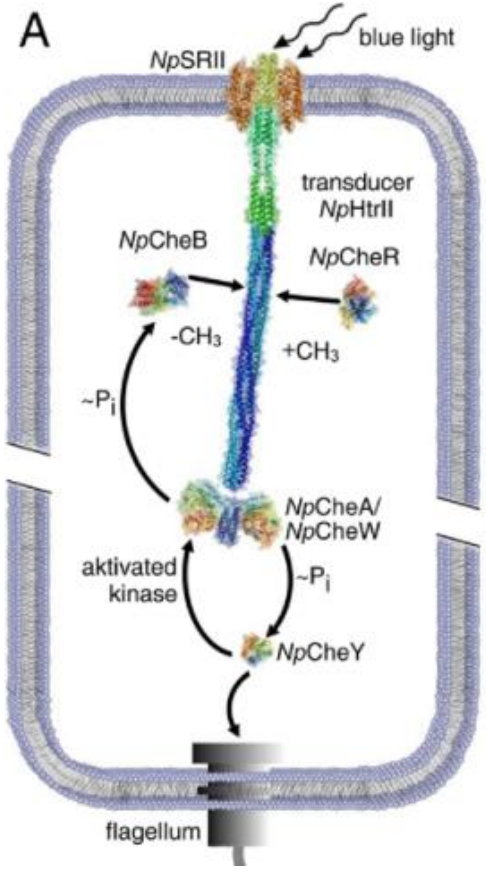

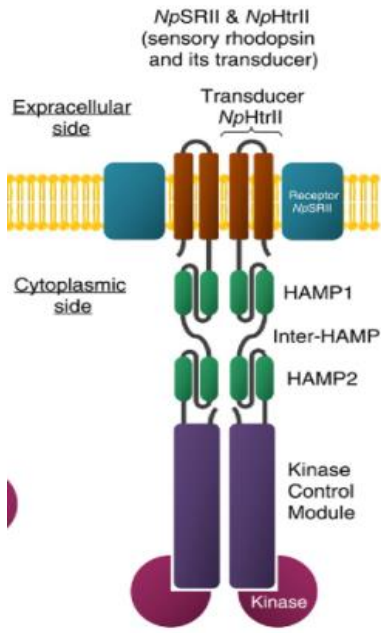

Soda Lake Zug from Wadi Natrun, Sahara Desert, Egypt

Grows optimally in 3.5 M NaCl and at pH 8.5.

- Signaling system
- Mediate phototaxis
- Extremely haloalkaliphilic archaeon

Ryzhykau, Y.L., Orekhov, P.S., Rulev, M.I. et al. Molecular model of a sensor of two-component signaling system. Sci Rep 11, 10774 (2021).

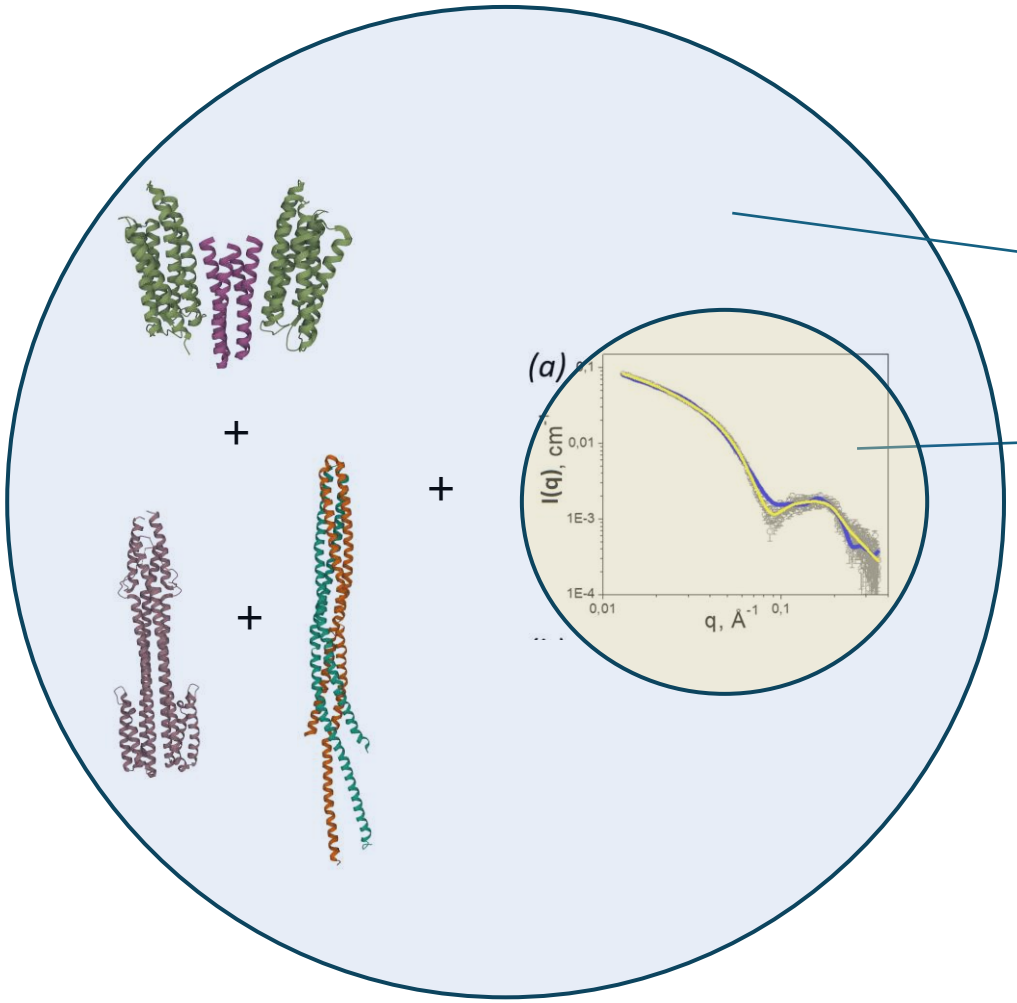

SAXS

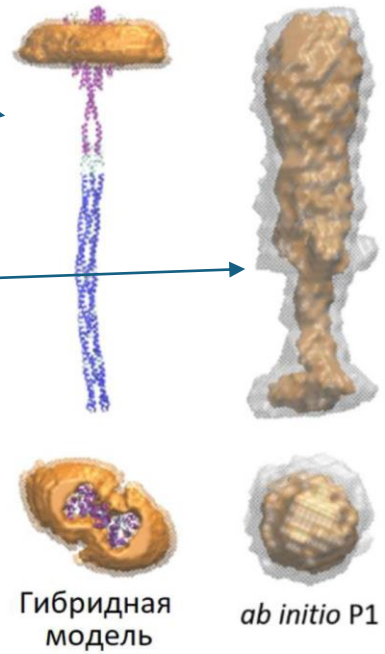

SANS

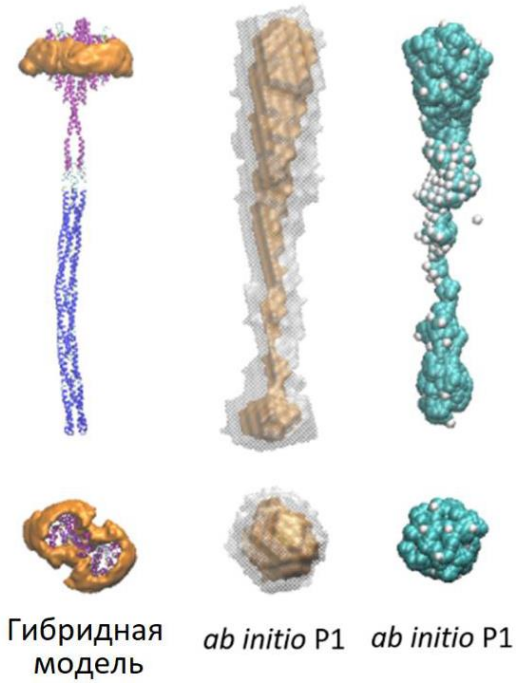

Ab initio models of *NpSRII/NpNtrII* complex at law ionic strength 150 mM NaCl
ATSAS program; MEMPROT

Ryzhykau, Y.L., Orekhov, P.S., Rulev, M.I. et al. Molecular model of a sensor of two-component signaling system. Sci Rep 11, 10774 (2021). https://doi.org/10.1038/s41598-021-89613-6

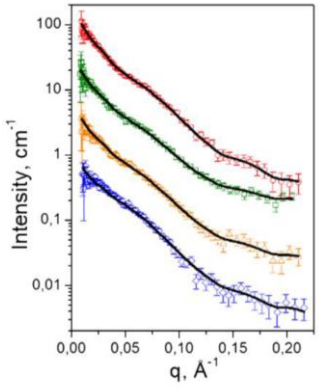

SANS experimental data obtained with the protein *Np*SRII/*Np*HtrII complex in D_2O solutions with 0.15, 1.4, 2.8 and 4.0 M NaCl

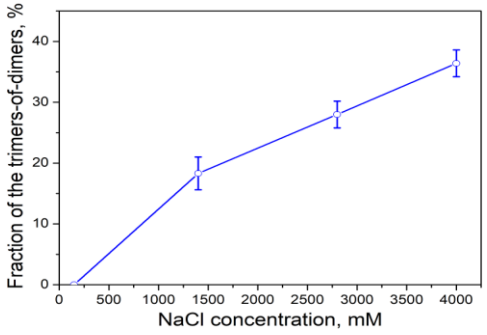

Weight fraction of the trimers of dimers of the full-length *Np*SRII/*Np*HtrII complex versus NaCl molarity. OLIGOMER program from ATSAS software suite. Fraction of the trimers-of-dimers at 150 mM NaCl assumed to be zero.

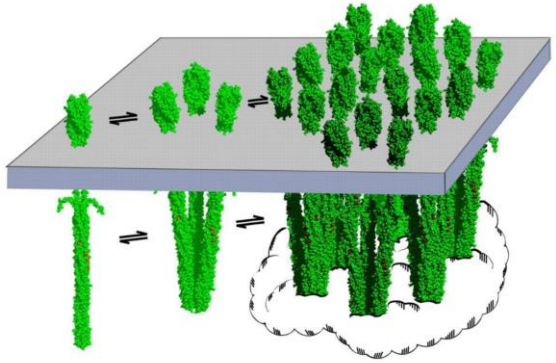

Oligomerization of dimers of chemoreceptors

Transmembrane-bound **Tripod-shaped**

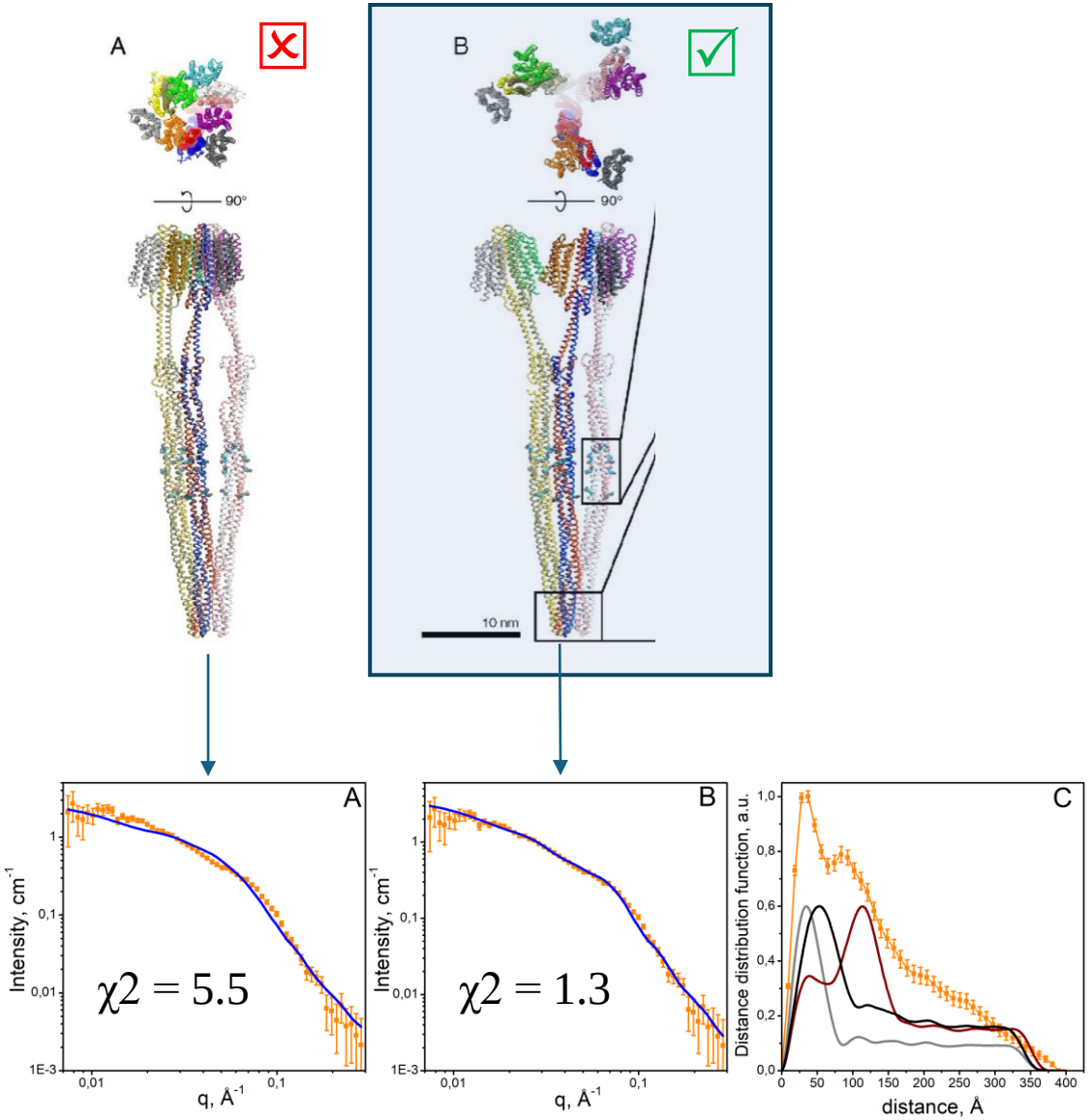

Ryzhykau, Y.L., Orekhov, P.S., Rulev, M.I. et al. Molecular model of a sensor of two-component signaling system. Sci Rep 11, 10774 (2021). https://doi.org/10.1038/s41598-021-89613-6

Contrast variation technique

$$I(q) = N(\Delta\rho V)^2 F(q)$$

$$\Delta\rho = (\bar{\rho} - \bar{\rho}_{buffer})$$

$$\rho = \sum_i b/V$$

Coherent scattering length for x-ray and neutron for main biological elements

Element/isotope	$b_{X\text{-ray}}$ (fm)	$b_{neutron}$ (fm)
Hydrogen (^{1}H)	2.82	−3.74
Deuterium (^{2}D)	2.82	6.67
Carbon (^{12}C)	16.9	6.65
Nitrogen (^{14}N)	19.7	9.36
Oxygen (^{16}O)	22.5	5.80
Phosphorous (^{31}P)	42.3	5.13

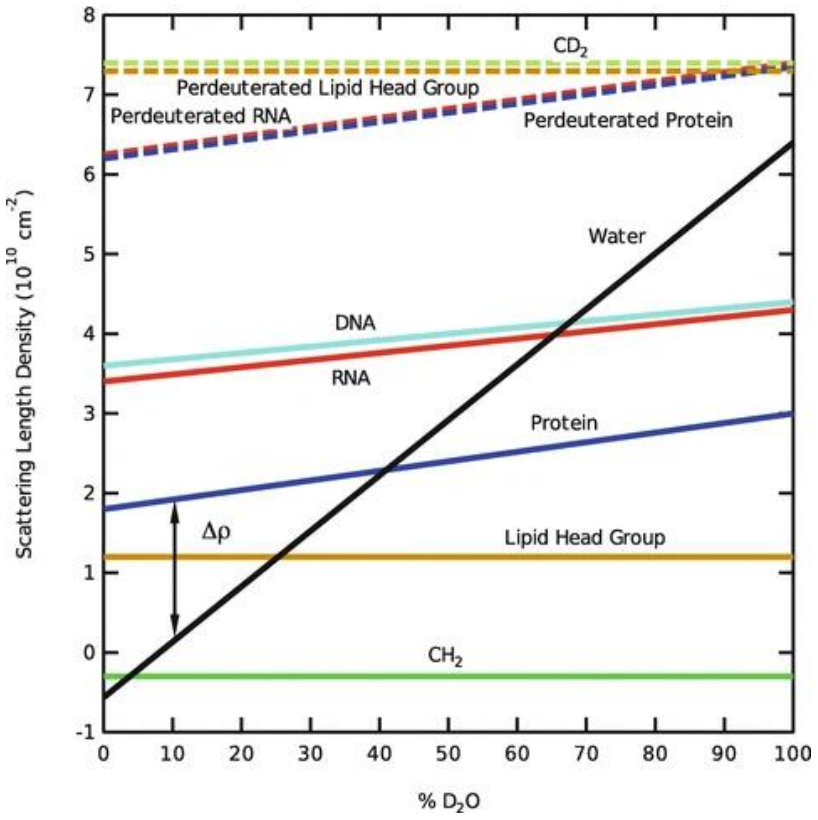

Zaccai NR, et al (2016). Methods in enzymology. Elsevier, pp 159–210

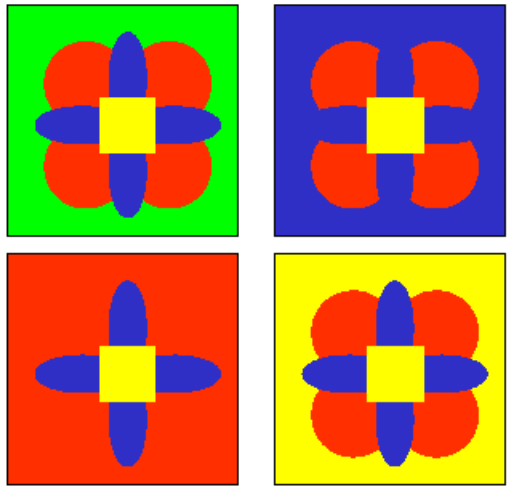

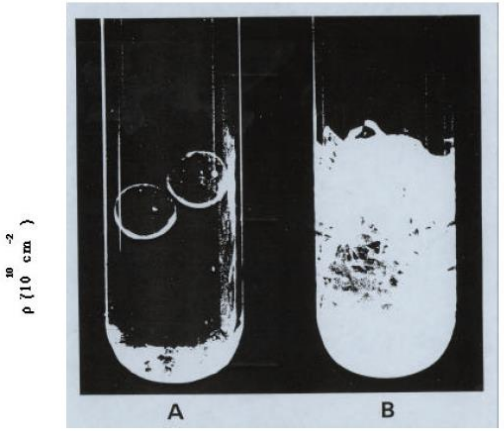

Tubes is borosilicate beads+pyrex fibers+solvent
A- refractive index matched to pyrex
B - solvent index different from beads and fibers

X-ray and neutron SLD for typical components of biological samples

Molecule	$\rho_{x\text{-ray}}$ e/Å3	$\rho_{neutron}$, 10-6 Å-2
H2O	0.334	-0.56
D2O	0.334	6.4
Protein	0.42	2.1
D-protein	0.42	6.6
Nucleic acid	0.55	3.7
D-Nucleic acid	0.55	6.6
Phospholipid	0.3	0.3
Phospholipid head (PC)		1.8
Phospholipid d-head (d-PC)		5.7
Phospholipid chain		-0.3
Phospholipid d-chain		7.0
Head phosphatidylglycerol (PG)		2.47
Head phosphatidylethanolamine (PE)		2.55
Hydrophobic region of DDM	0.275	-0.4
Hydrophilic region DDM group of DDM	0.515	3.9

Objects for contrast variation technique

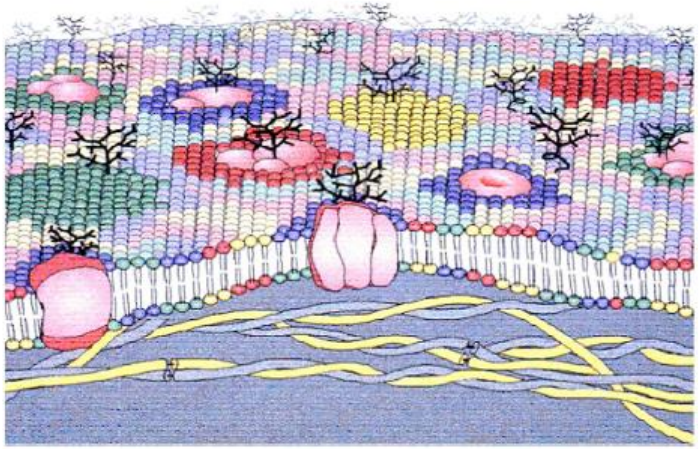

Biological membranes

Escribá et al., JCMM (2008)

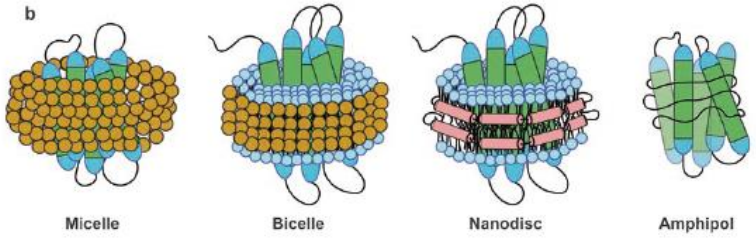

Ishchenko, A. et al. (2017) Protein Crystallography. Methods in Molecular Biology, vol 1607.

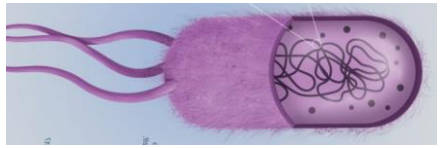

bacteria

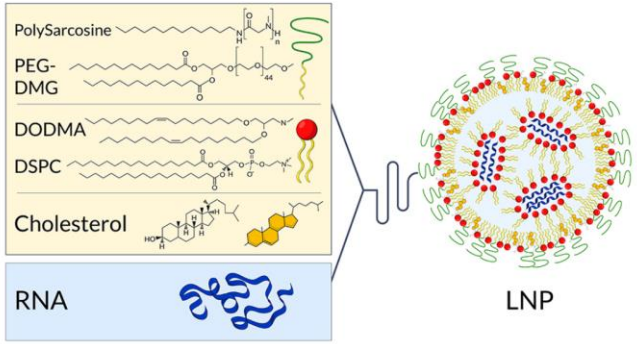

vaccine

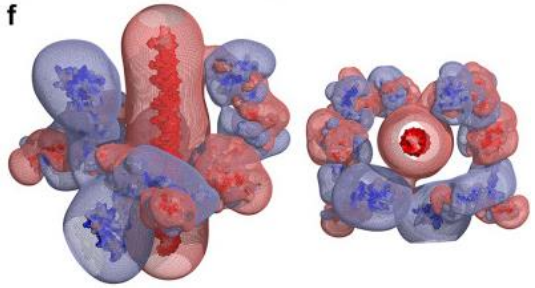

DNA+protein complex

Cellular organelles

Supramolecular organization of the visual pigment rhodopsin

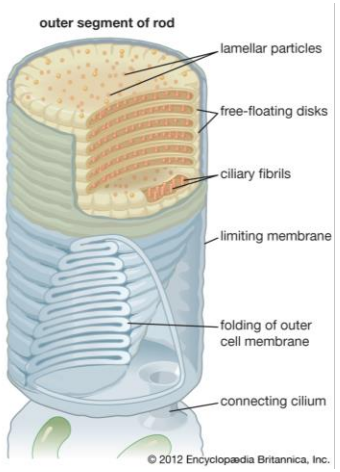

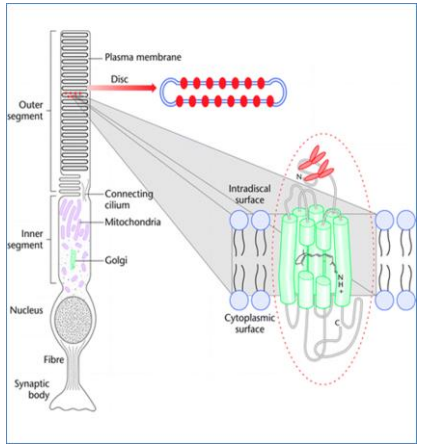

AFM of outer shape of disc with the rhodopsin protein from rod cell

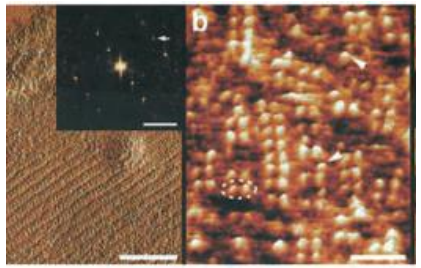

Distance between rhodopsin centers 38 Å.
Rhodopsin molecule size is 35 Å.

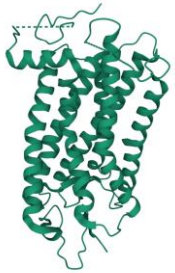

CRYSTAL STRUCTURE OF BOVINE RHODOPSIN PDB 1F88

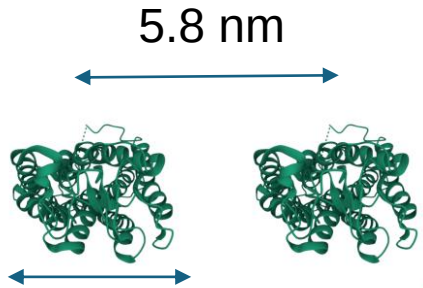

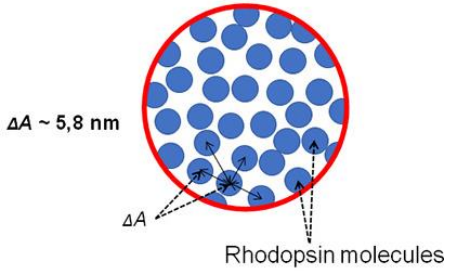

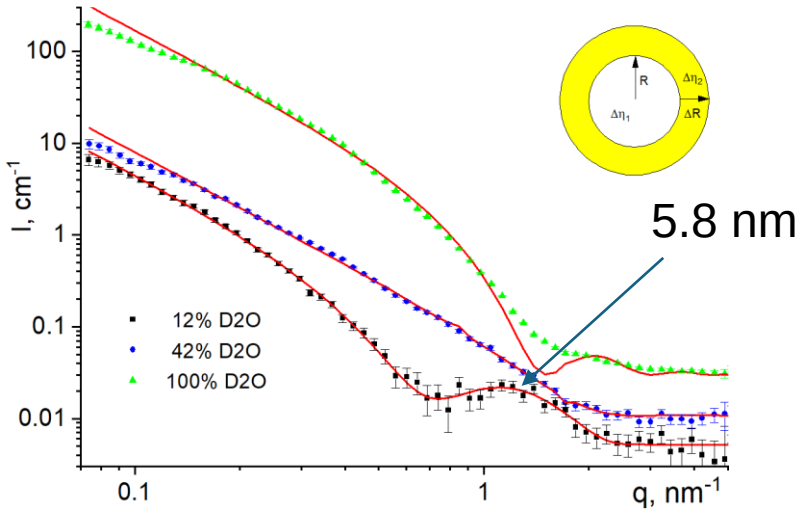

Photoreceptor disk Rot outer segment

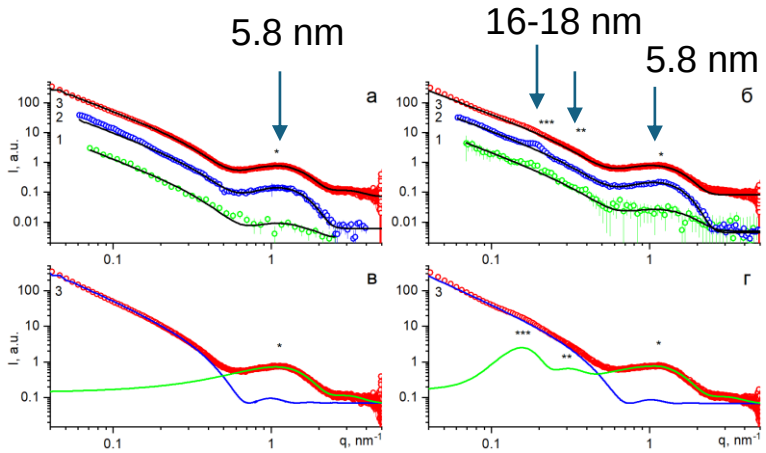

T. B. Feldman, Oleksandr I. Ivankov, Alexander I. Kuklin, Tatiana N. Murugova, et al. // Biochimica et Biophysica Acta (BBA) – Biomembranes (2019), 1861

Membrane proteins:
How to deal with the detergent belt - Masking out

1. Mix D2O / H2O in a buffer

2. Mix of h-detergent / d-detergent
+ deuterated proteins

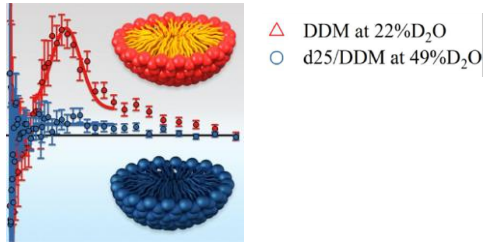

R. C. Oliver et. al. // *The Journal of Physical Chemistry Letters* **2017** *8* (20), 5041-5046

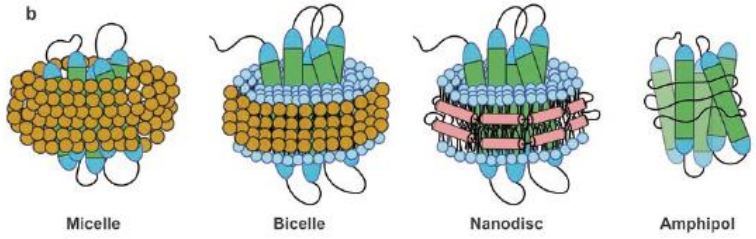

3. The synthesis of isotope-substituted detergents to have match-out at 100% D2O

Table 1. Deuteration levels needed and obtained for *n*-octyl β-D-glucopyranoside (OG) and *n*-dodecyl-β-D-maltopyranoside (DDM).

	OG		DDM	
	Head group	Tail group	Head group	Tail group
Chemical composition of the detergent component	$C_2H_{11}O_6$	C_8H_{17}	$C_{12}H_{21}O_{11}$	$C_{12}H_{25}$
Exchangeable hydrogens	4	0	7	0
Theoretical level of deuteration needed for match-out at 100% D_2O	$C_6D_{7.6}H_{3.4}O_6$	$C_8D_{15.9}H_{1.1}$	$C_{12}D_{15.2}H_{5.8}O_{11}$	$C_{12}D_{22.4}H_{2.6}$
Experimentally obtained level of deuteration in 100% D_2O	$C_6D_{7.64}H_{3.36}O_6$	$C_8D_{15.98}H_{1.12}$	$C_{12}D_{14.98}H_{6.02}O_{11}$	$C_{12}D_{22.25}H_{2.75}$

Midtgaard, S.R., et al. // (2018), FEBS J, 285: 357-371

4. Production of lipids and scaffold proteins in a host organism in D2O-media to have match-out at 100% D2O

Difficulties:

- Limited availability of d-detergents
- Difficulties in the expression and purification of d-proteins
- High cost

How to deal with the detergent belt: Hybrid approach

PDB protein-structure + coarse-grained detergent belt structure

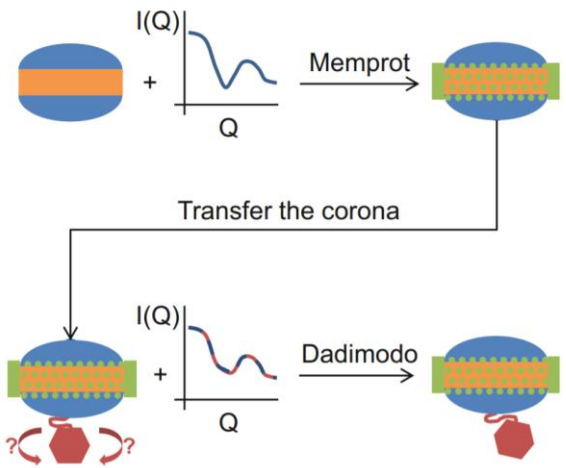

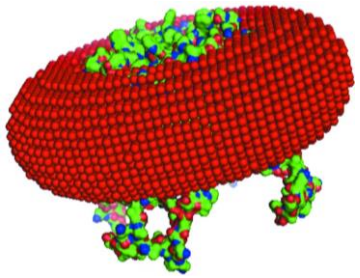

Geometrical representation nano-disc + coarse-grained protein shape

Top and side view of one particular result of an *ab initio* analysis of the scattering data. The phospholipid head and tail groups of the nanodisc are represented by the blue and yellow discs, respectively. The belt protein is not shown.

Baranowski M., Pérez J. (2020) In: Biophysics of Membrane Proteins. Methods in Molecular Biology, vol 2168. Humana, New York, NY.

Pérez J, Koutsioubas A. Memprot: a program to model the detergent corona around a membrane protein based on SEC-SAXS data. Acta Crystallogr D Biol Crystallogr. (2015) 1;71(Pt 1):86-93.

Skar-Gislinge N, Kynde SA, Denisov IG, et al. *Acta Crystallogr D Biol Crystallogr*. 2015;71(Pt 12):2412-2421. doi:10.1107/S1399004715018702

Ab initio models from contrast variation

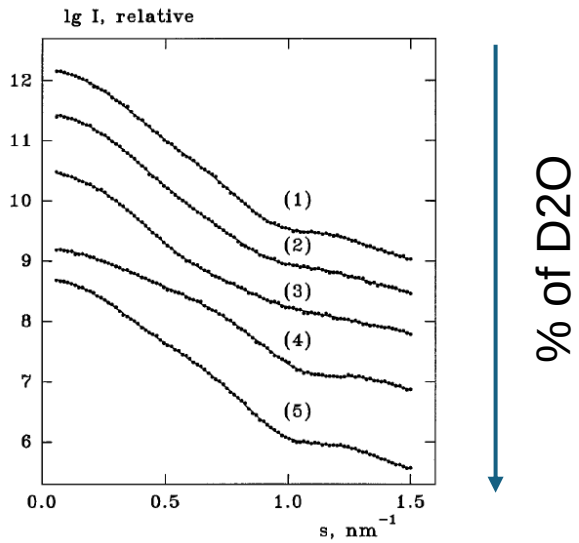

% of D2O

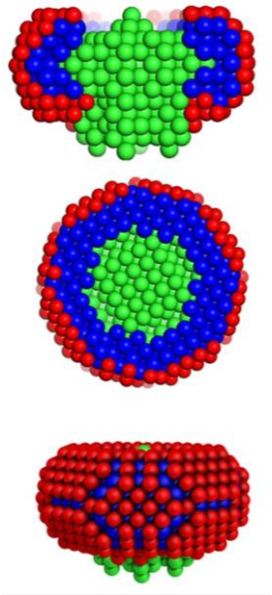

MONSA (multi-phase *ab initio*, the model was built from precalculated searching volume; fourfold symmetry around *z*-axis is imposed)

Molodenskiy, D.S., Mertens, H.D.T. & Svergun, D.I. An automated data processing and analysis pipeline for transmembrane proteins in detergent solutions. *Sci Rep* **10,** 8081 (2020).

MD structure

SANS curves with imposed fourfold axial symmetry

Ab initio shape reconstructions of the 270 dDM/AQ0 tetramer. The bead colors correspond to *green*, protein; *cyan*, detergent hydrophilic heads; and *magenta*, detergent hydrophobic tails.

Koutsioubas, Alexandros // Biophysical Journal, Volume 113, Issue 11, 2373 - 2382

Study of the structure of live functioning mitochondria (SANS experiments)

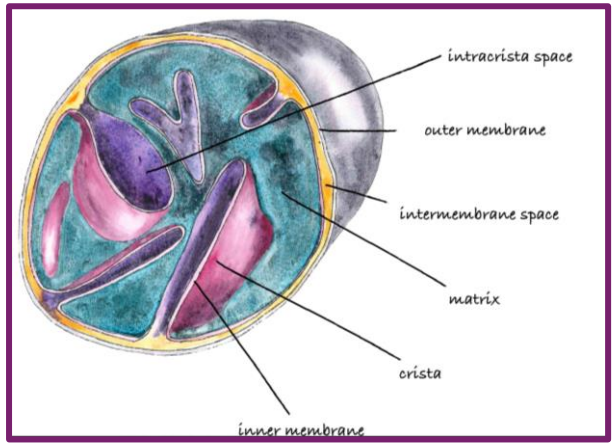

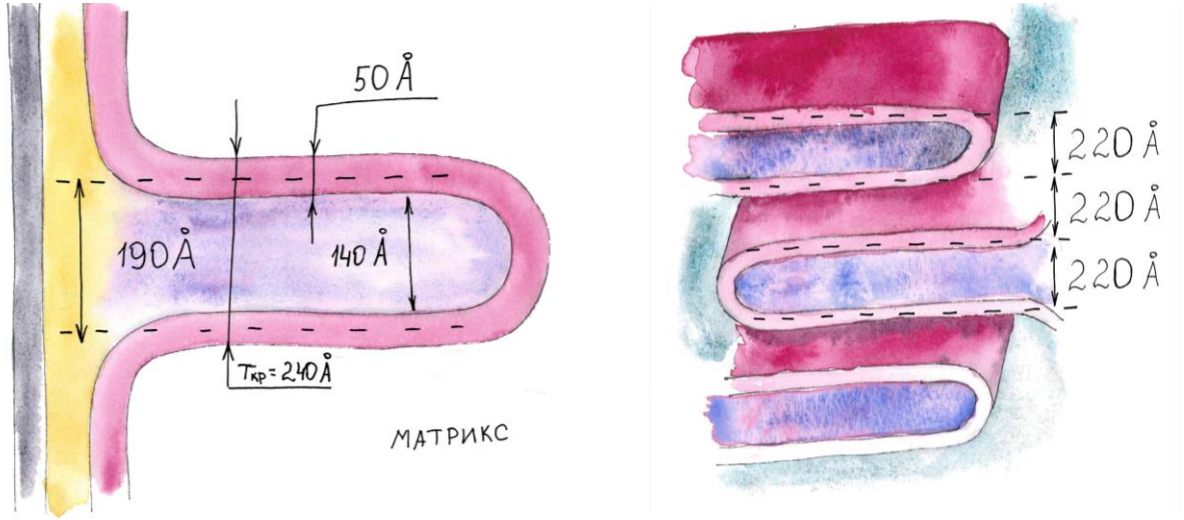

Structure of a liver mitochondrial crista under conditions of matrix swelling (hypotonic conditions),
and heart mitochondrial cristae in normal (isotonic) conditions

Structure of rat heart mitochondrial cristae in hypotonic conditions.

Murugova, T. N., et al. Neutron News 22 (2011).

Byvshev, I. M., et al. Biophysics 63 (2018).

Other scattering methods

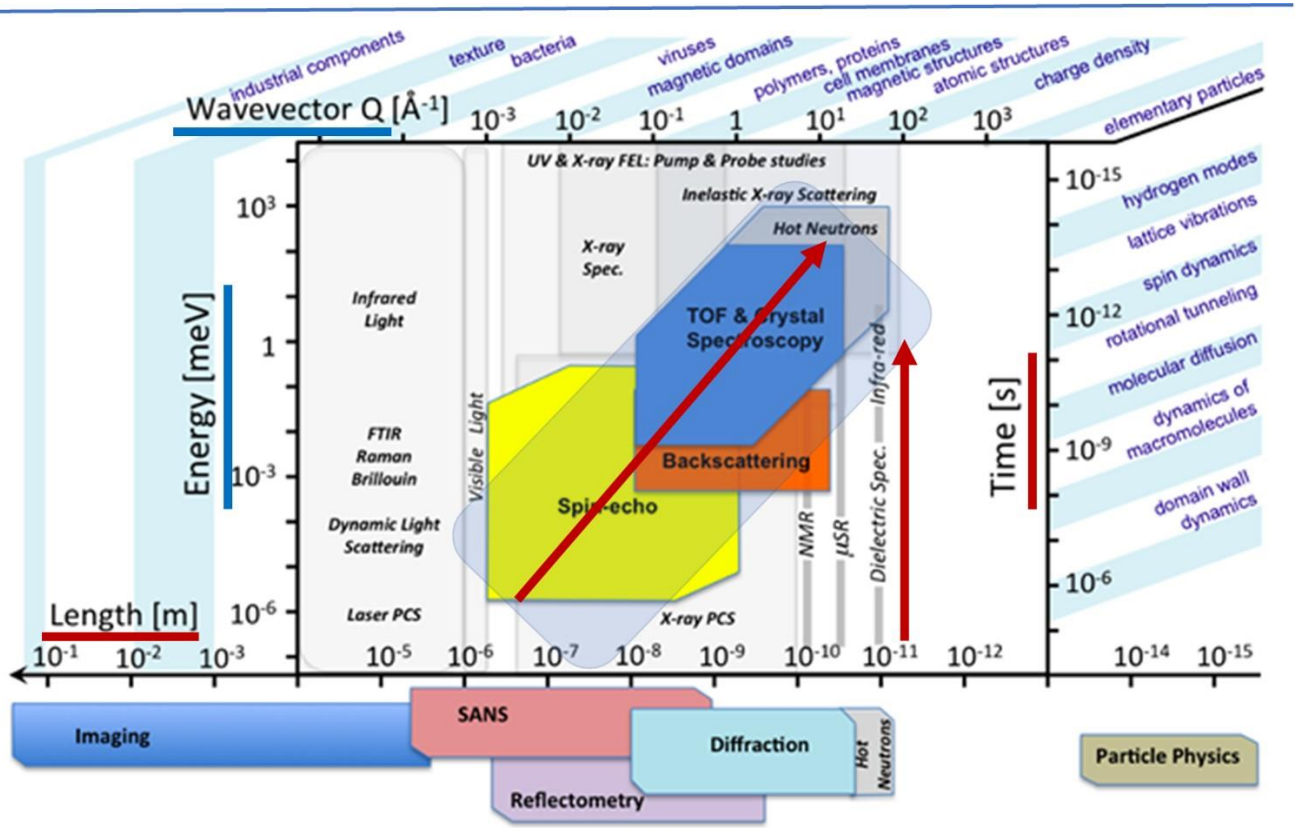

spectroscopy

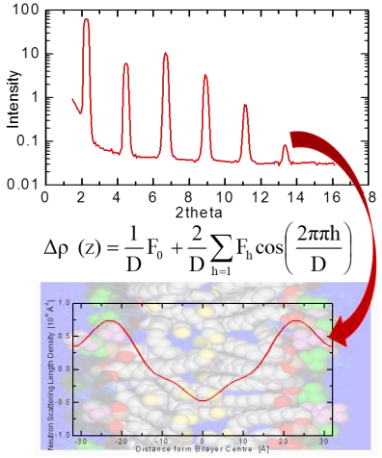

Diffraction

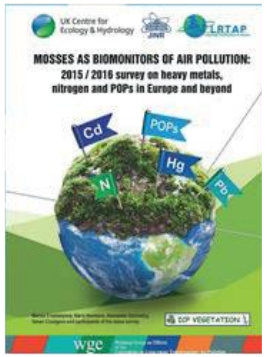

Neutron activation analysis

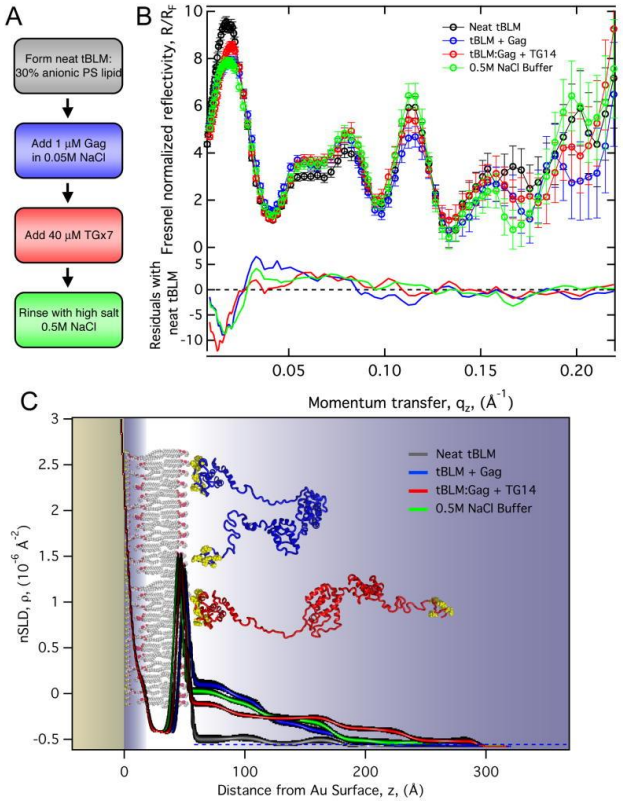

Reflectormetry

Datta SA, et al. HIV-1 Gag extension: conformational changes require simultaneous interaction with membrane and nucleic acid. J Mol Biol. 2011 Feb 18;406(2):205-14.

Thank you for your attention!

Acknowledge:

A. Ivankov and N. Kucerka for help in preparing some slides for this presentation